Scattering of thermal He beams by crossed atomic and molecular beams. V. Anisotropic intermolecular potentials for $He+CO_2$, N_2O, C_2N_2 [a)]

Gregory A. Parker,[b)] Mark Keil,[c)] and Aron Kuppermann

Arthur Amos Noyes Laboratory of Chemical Physics,[d)] California Institute of Technology, Pasadena, California 91125

(Received 4 February 1982; accepted 25 June 1982)

Experimentally measured differential cross sections are presented for the interactions of He with the linear molecules CO_2, N_2O, and C_2N_2. These data show pronounced dampening of the diffraction oscillations, and provide an indication that the intermolecular potentials have large anisotropies. Indeed, central-field analyses of the experimental data, even in terms of very flexible models, are shown to be inadequate. However, an anisotropic analysis using the infinite-order sudden approximation yields physically reasonable intermolecular potentials, and provides excellent fits to the scattering data. Neither the spherical averages of these empirical anisotropic potentials, nor the spherically symmetric potentials obtained by the central-field analyses, reproduce the experimental differential cross sections. For $He + CO_2$, the anisotropic potential is extended to highly repulsive interactions, to which the present data are insensitive, by combining theoretical calculations and measurements of gas-phase bulk properties. Estimates for the reliability of the fitted anisotropic potentials are given, and convenient parametrizations are recommended.

I. INTRODUCTION

Molecular scattering data have been very useful in the determination of intermolecular potentials, particularly if the species are spherically symmetric, or nearly so.[1-4] Using central-field potentials to analyze experimental data for anisotropic systems is predicated on the assumptions that (a) anisotropic contributions to the intermolecular potential are negligible within the sensitivity of the scattering experiments and/or that (b) the total (i.e., unresolved inelastic plus elastic) differential cross section for scattering in anisotropic systems is sensitive only to the spherical average of the (actual) anisotropic potential. However, these assumptions have been shown, by way of specific examples, to be invalid for scattering of highly anisotropic systems,[5,6] or at very low collision energies.[7]

Semiclassical[8] and quantal[6,9] theories have been used to predict quenching of the various oscillatory structures of differential and integral cross sections[10] for anisotropic interactions; these effects have also been observed experimentally.[4(a),5,11-13] Despite fundamental interest in molecular anisotropies, detailed experimental investigations have only recently been successful in investigations of interaction asphericities.[14-18] However, only a few studies have directly yielded information about the anisotropic intermolecular potential, especially in the vicinity of the important van der Waals minimum.[5,13(b),15(a),17(a),19]

With the recent success of rotational decoupling approximations,[6,20] it is now possible to routinely determine a wide variety of phenomenological cross sections, without having to perform elaborate close-coupling calculations.[6,20-24] In particular, the infinite-order sudden approximation (IOSA), which totally decouples the rotations, gives rise to simplified expressions for these phenomenological cross sections.[6,20(a),25-28]

In the present paper we analyze experimental measurements of the total (elastic plus inelastic) differential cross sections (DCS) for the highly quantum and anisotropic systems $He + CO_2$, N_2O, and C_2N_2, obtained using room temperature crossed molecular beams. In Sec. II, we show why and how the IOSA can be used, with existing central-field data reduction programs,[3(b)] to determine anisotropic intermolecular potentials. In Sec. III, we present our experimental results, and the procedures used in the data reduction. Central-field and anisotropic potential forms used for the data analyses are given in Sec. IV. In Sec. V, we present empirical anisotropic intermolecular potentials, and discuss the *inappropriateness* of the central-field analysis for the systems considered in this study. We pay particular attention to the $He + CO_2$ potential, discussing the sensitivity with which its parameters can be determined from total DCS measurements. Electron-gas calculations are also used to extend this anisotropic potential to highly repulsive intermolecular interactions to which the DCS data are insensitive. We also compare our calculated second virial, diffusion, viscosity coefficients, and total integral cross sections, with available experimental results. Finally, we summarize our results in Sec. VI.

II. THEORY

A detailed description of the infinite-order sudden approximation (IOSA) has been given elsewhere,[6] and we will only briefly discuss the theory to show *how* it can be used to obtain anisotropic intermolecular potentials. We assume that the molecular target is a linear rigid

[a)]This work was supported in part by the U. S. Department of Energy, Contract No. DE-ASO 3-76SF00767; Project Agreement No. DE-ATO 3-76ER72004. Report Code: CALT-767P4-182.

[b)]Present address: Department of Physics and Astronomy, University of Oklahoma, Norman, Oklahoma 73019.

[c)]Present address: Department of Chemistry, University of Alberta Edmonton, Alberta T6G 2G2, Canada.

[d)]Contribution No. 6562.

 0021-9606/83/031145-18$2.10

rotor, since at the collision energies used, vibrational transitions are inaccessible. We define our coordinate system such that r is the length of the position vector r of the atom with respect to the molecular center-of-mass, and γ is the angle between r and the molecular axis. The Hamiltonian for an S-state atom interacting with a Σ-state rigid rotor is

$$H = -\frac{\hbar^2}{2\mu r}\frac{\partial^2}{\partial r^2} r + \frac{\mathfrak{L}^2}{2\mu r^2} + \frac{\mathfrak{J}^2}{2I} + V(r,\gamma) , \tag{1}$$

where μ and $\mathfrak{L}$ are the reduced mass and orbital angular momentum, respectively, of the atom relative to the molecule. The total angular momentum J is the sum of the molecular angular momentum $\mathfrak{J}$ and the orbital angular momentum $\mathfrak{L}$,

$$\mathbf{J} = \mathfrak{J} + \mathfrak{L} . \tag{2}$$

The moment of inertia of the rigid rotor is I and $V(r,\gamma)$ is the interaction potential. In the IOSA, one makes both the centrifugal sudden[29,30]

$$\mathfrak{L}^2 \simeq \hbar^2 l(l+1) \tag{3}$$

and energy sudden[31]

$$\mathfrak{J}^2 \simeq \hbar^2 j(j+1) \tag{4}$$

replacements of the angular momentum operators[20(a)] by their respective eigenvalue forms. For a rigid rotor, this results in an uncoupled set of ordinary differential equations

$$\left[\frac{d^2}{dr^2} + k^2 - \frac{l(l+1)}{r^2} - \frac{2\mu}{\hbar^2} V(r,\gamma)\right] g_l(r;\gamma) = 0 , \tag{5}$$

to be solved for the radial wave functions $g_l(r;\gamma)$, subject to the usual scattering boundary conditions

$$g_l(0;\gamma) = 0 \tag{6}$$

and

$$[g_l(r;\gamma) \underset{r\to\infty}{\sim} k^{-1/2}(\exp[-i(kr - l\pi/2)] - \exp\{i[kr - l\pi/2 + 2i\eta_l(\gamma)]\})], \tag{7}$$

where $\eta_l(\gamma)$ is the phase shift for a *fixed* orientation angle γ. The wave number k,

$$k^2 = \frac{2\mu}{\hbar^2}\left[E - \frac{\hbar^2 j(j+1)}{2I}\right], \tag{8}$$

is a measure of the incident relative kinetic energy.

The IOSA is accurate when two conditions are satisfied: (1) the relative kinetic energy is large compared to the rotational energy level spacing (energy sudden approximation), and (2) rotational transitions are dominated by low values of the orbital angular momentum, i.e., small impact parameters (centrifugal sudden approximation). For the systems studied in this paper, the collision energy used (~ 64 meV) is substantially larger than the separation between adjacent rotational energy levels. For the most populated state, at 300 K, this spacing is ~ 3 meV, so that the first condition is satisfied. Validity conditions suggest that the centrifugal sudden approximation will be valid when the well depth is substantially less than the collision energy, both before and after the collision.[20(a)] This condition is thus also satisfied for the elastic and inelastic collisions studied in this paper (except those very near threshold, with concomitantly small cross sections) since well depths for He-molecule systems are generally 5 meV or less.[2-5,32]

As shown elsewhere,[6,33] the "total" (elastic plus inelastic) DCS is simply the weighted orientation average

$$\sigma(\theta) = \frac{1}{2}\int_0^{\pi} \sigma(\gamma,\theta)\sin\gamma\, d\gamma \tag{9}$$

of the central-field DCS's

$$\sigma(\gamma,\theta) = \frac{1}{4k^2}\left\{\left[\sum_{l=0}^{\infty}(2l+1)\sin[2\eta_l(\gamma)]P_l(\cos\theta)\right]^2 + \left[\sum_{l=0}^{\infty}(2l+1)(\cos[2\eta_l(\gamma)]-1)P_l(\cos\theta)\right]^2\right\}. \tag{10}$$

In deriving this simplified expression, it was necessary to neglect the velocity changes of rotationally inelastic collisions, which is consistent with the IOSA. Pack and Preston[33] have shown that with this assumption the center-of-mass to laboratory coordinate transformation is identical to that for central-field elastic scattering. We could thus adapt the central-field data reduction procedure (Sec. III), with only the relatively minor modifications needed to include anisotropic effects [Eq. (9)], to perform the appropriate incident velocity and beam angle averaging, for direct comparisons with the experimental DCS's presented below. Rotzoll and Lübbert found[34] that this hypothesis is valid for $He + CO_2$ scattering but is invalid for $Ar + CO_2$ scattering.

III. EXPERIMENTAL AND DATA REDUCTION

The crossed molecular beam apparatus has been discussed previously,[3] so that only a brief outline of its major features is given here. A modulated He beam is formed in a supersonic expansion, and is angularly well collimated in two stages of differential pumping. Secondary beams of the various gases studied emerge directly into the scattering chamber through a glass capillary array. The secondary beam source may be tilted upwards, thus uncrossing the beams, for measurements of background scattering intensity. Beam operating characteristics are summarized in Table I. Due to the slightly supersonic nature of the secondary beam, its internal temperature (particularly the rotational temperature) may not be the ambient one (298 K). We note that its velocity distribution is best characterized by a Mach number of 1.5 (Table I) and an "effective" specific heat ratio of 1.64, the latter indicating cooling of only the transverse translational degrees of freedom.[35] Because the secondary beam particles are much heavier than those of the primary for all the scattering experiments considered in this study, the rather wide velocity distribution of the secondary beam does not contribute significantly to the distribution of relative collision velocities; the overall apparatus velocity resolution is only slightly poorer than that of the highly supersonic He beam.

As in earlier work, a quadrupole mass spectrometer is used to detect out-of-plane scattering of He atoms as a function of the scattering angle (with the in-plane scattering angle fixed at 0°). Ion detection and signal pro-

TABLE I. Beam operating conditions.

Characteristic	Primary beam	Secondary beams		
Beam gas	He	CO_2	N_2O	C_2N_2
Inlet pressure/Torr	1300	4.1	4.1	4.1
Inlet temperature/K	298	298	298	298
Angular FWHM[a]/deg	1	4	4	4
Most probable velocity/(km/s)	1.757	0.478	0.478	0.440
Velocity FWHM,[a] $\Delta v/v$	0.10	0.75	0.75	0.75
Mach number[b]	18	1.5	1.5	1.5

[a]Full width of half-maximum. [b]Reference 35.

cessing utilizes a Spiraltron continuous dynode electron multiplier. Its pulses are sufficiently fast ($\lesssim 1$ μs) to allow use of digital counting techniques; the gates of an up-down counter are synchronized with the primary beam chopper.

Differential pumping in the mass spectrometer is provided by a small (5 l/s) ion pump in the detector entrance buffer chamber, followed by a larger (25 l/s) ion pump in the ionizer region. During experiments, we also use a liquid helium cryopump (400 l/s), which provides effective pumping, even for He!$^{3(b)}$ The pressure in the ion source region was $\sim 1\times10^{-9}$ Torr during the course of these experiments.

Rapid cryopumping of the CO_2 and C_2N_2 beams on liquid-nitrogen cooled surfaces kept the scattering chamber pressure at $\sim 3\times10^{-7}$ Torr, while use of the less condensable N_2O beam raised this pressure to $\sim 1\times10^{-6}$ Torr. These pressures, coupled with a primary beam attenuation due to scattering by the secondary beam of only ~5%, easily ensure that the single-collision conditions essential for DCS measurements prevail. Periodic mass spectrometric checks of the secondary beams revealed their high purity for all the scattering experiments, with no discernible dimerization.

Scattered primary beam signals were measured between ~2° and ~20° above the plane of the beams, at a relative collision energy of ~64 meV (the exact values depend on the identity of the secondary beam gas). Measurements were also made for out-of-plane scattering below the plane of the beams, in order to locate accurately the zero position of the angular scattering scale (to within ~0.03°).$^{3(b)}$ Long-term drifts in beam intensities and detection efficiency were compensated for by periodic measurements of the scattered signal at a reference angle near 5°. The experimental DCS's are shown in Fig. 1 for $He+CO_2$, $He+N_2O$ and $He+C_2N_2$.^{36} Data points represent the average of three or four independent angular scans performed in several days' experimentation for each scattering pair. Total counting times at each angle ranged from ~3 min at 2°, to ~30 min at 20°. Signal-to-noise ratios over the same angular range were between about 50 and 5, respectively.

The data reduction procedure used to obtain the fits shown in Fig. 1 has also been described previously.$^{3(b)}$ We use Marquardt's^{37} weighted least-squares prescription to fit the parameters of mathematical functions chosen to represent the intermolecular potential, as discussed in Sec. IV. DCS's in the center-of-mass coordinate frame are calculated from partial wave phase shifts of high accuracy, and are then averaged over both beams' angular and velocity spreads in the transformations to the out-of-plane laboratory coordinate frame. The overall apparatus velocity resolution is

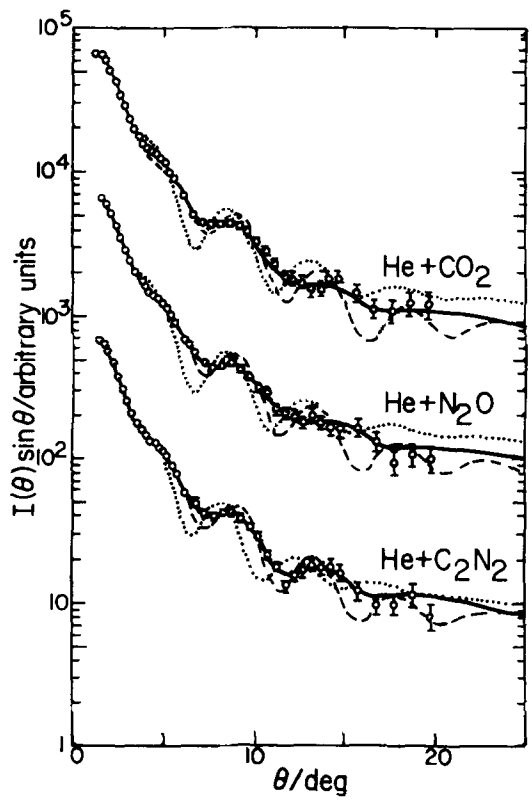

FIG. 1. Laboratory differential cross sections for out-of-plane scattering of He by CO_2, N_2O, and C_2N_2, with ordinates shifted downwards by one decade for each system in this sequence. Points with error bars are the experimentally measured scattering cross sections (Ref. 36) $I(\theta)\sin\theta$ vs the scattering angle θ, for a collision energy of 64 meV. Curves are DCS's calculated using intermolecular potentials extracted from the data. Solid curves: anisotropic MSV parameter expansion potentials of Eqs. (14)–(16); dashed curves: central-field SPFD potentials; dotted curves, spherical averages of the anisotropic MSV potentials.

~11% FWHM for the systems included in this study. Averaging is also used to account for the overall apparatus angular resolution of 1.9° FWHM.

The fitting quality for the calculated DCS's (relative to the experimental ones) are expressed as χ^2 or as $\Delta\alpha/\alpha$ statistical indices.[3(b)] The former is the sum of weighted residuals squared, which is the quantity minimized by the weighted least-squares fits. The latter gives the 95% confidence level[38] for the scaling factor α necessary to bring the calculated (absolute) cross sections into vertical register with the experimental (arbitrarily normalized) intensities.[36] The $\Delta\alpha/\alpha$ goodness-of-fit index is statistically adjusted both for the number of data points, and for the number of parameters varied in the fits. Furthermore, it is independent of the arbitrary normalization used in the experiments, and is a more useful index than χ^2 for comparing fitting quality between different experiments or potential fits.[3(b)]

IV. DATA ANALYSIS AND INTERMOLECULAR POTENTIALS

The experimental DCS's obtained as described in Sec. III and displayed in Fig. 1, were fitted by weighted least-squares optimization of the parameters of the various intermolecular potentials described below. These included both central-field and anisotropic models.

A. Central-field potential models

The van der Waals interactions for the atom–molecule systems considered in this study are anisotropic. As such, central-field potentials, represented generically by

$$V(r) = \epsilon \cdot f(\rho) , \quad \rho = \frac{r}{r_m} , \tag{11}$$

where r_m is the radius of the attractive minimum and ϵ is its depth, provide at best an approximate description of these interactions.[4(a)] For a thermal rigid rotor at 300 K, representative of the secondary beams used in the present studies (Sec. III), a typical rotation frequency is $\sim 3\times10^{11}$ Hz. Since the collision interaction time (to traverse ~10 Å) is $\sim 6\times10^{-13}$ s, the molecule rotates too slowly to establish an effective isotropic potential. Central-field analyses therefore were performed herein to test the validity of the approximation of Eq. (11).

To assure that the above test would be independent of the particular parametrization chosen, we used a variety of central-field potentials, some of which were highly flexible. Both the double-Morse-spline-van der Waals (M^2SV)[39] and third-order Simons–Parr–Finlan Dunham (SPFD)[40,41] parametrizations have sufficient flexibility to mimic realistic central-field potentials. In fits to the present experiments, the small statistical parameter correlations observed indicate that five of their parameters may be determined by fitting to room temperature DCS data from highly quantum interactions.[42] We also used four parameters of the Morse-spline-van der Waals (MSV)[43] potential form to fit just the low-angle ($\theta \lesssim 6°$) portion of the DCS's presented here (see Sec. V). Finally, the Hartree–Fock-dispersion (HFD) potential form[44] was used due to its success in fitting central-field atom–atom scattering data. As used in this study, the HFD potential had just one adjustable parameter.

B. Anisotropic potential models

For a more realistic analysis of the experimental DCS's, we used several anisotropic potential forms. These differ not only in the parametrization of the radial dependence of the potential energy, but also in the way the anisotropy is introduced into the potential. Using several physically reasonable potential forms in this manner enables us to evaluate the uniqueness and reliability of the resulting anisotropic intermolecular potentials. At present, this seems to be a necessary procedure in fitting anisotropic potentials, since their form is not yet as well understood[14,45] as for central-field potentials.[46]

We note that potential models for $He+CO_2$ and $He+C_2N_2$ should reflect the $D_{\infty h}$ symmetry of the molecular partner. For $He+N_2O$, we may hope that the lower $C_{\infty v}$ molecular symmetry is of rather small consequence. For example, the molecular center-of-mass almost coincides with the geometric center (within 0.03 Å), and the dipole moment is only 0.167 D.[47] Our anisotropic potential models therefore were based on $D_{\infty h}$ molecular symmetry, even for $He+N_2O$.

1. *Legendre expansion potentials*

The mathematical form most commonly used in studies of anisotropic intermolecular potentials is a Legendre polynomial expansion of the potential:

$$V(r,\gamma) = \sum_{n=0}^{\infty} V_n(r) P_n(\cos\gamma) . \tag{12}$$

Since several parameters are needed to specify each of the $V_n(r)$ (spherically symmetric) potential terms, there would be an unwieldy number of parameters for expansions beyond $n=2$. For any particular Legendre expansion potential, the $V_0(r)$ and $V_2(r)$ potential parametrizations used were the same, though of course one pair of r_m and ϵ parameters were used for the $V_0(r)$ term, while a distinct pair were used for the $V_2(r)$ term. We usually used just one shape parameter for both $V_0(r)$ and $V_2(r)$ terms, but in some cases even the shape parameters were fit independently.

2. *Multicenter potentials*

The second mathematical form used to construct anisotropic potentials expresses them as the sum of three central-field potentials, with centers located along the molecular axis,

$$V(r,\gamma) = V_c(r) + V_e(x_1) + V_e(x_2) ,$$

where

$$x_1 = [r^2 + (z^2/4) - rz\cos\gamma]^{1/2} \tag{13}$$

and

$$x_2 = [r^2 + (z^2/4) + rz\cos\gamma]^{1/2} .$$

In these equations, the molecular center-of-mass is the

TABLE II. Parametrizations used to construct anisotropic potential models.

Type	Mathematical form		Parameters
LJ	$V(r)=\epsilon\left(\frac{r_m}{r}\right)^6\left[\left(\frac{r_m}{r}\right)^6-2\right]$		r_m, ϵ
HFD	$V(r)=\begin{cases}\epsilon\exp[-\beta r_m^{-1}(r-r_m)]-\left[\frac{C_6}{r^6}+\frac{C_8}{r^8}\right]\exp[-(1.28r_m/r-1)^2] & r<1.28\,r_m \\ \epsilon\exp[-\beta r_m^{-1}(r-r_m)]-\left[\frac{C_6}{r^6}+\frac{C_8}{r^8}\right] & r>1.28\,r_m\end{cases}$		r_m only; $\epsilon=0.46(C_6r_m^{-6}+C_8r_m^{-8})$; $\beta=0.92\epsilon^{-1}(6C_6r_m^{-7}+8C_8r_m^{-9})-1.43$; C_6, C_8 are fixed (Table III)
LJ8	$V(r)=\frac{2\epsilon r_m^{12}-\frac{1}{2}C_6r_m^6}{r^{12}}-\frac{C_6}{r^6}-\frac{3\epsilon r_m^8-\frac{3}{2}C_6r_m^2}{r^8}$		r_m, ϵ, C_6
Morse	$V(r)=\epsilon\exp[-\beta r_m^{-1}(r-r_m)]\{\exp[-\beta r_m^{-1}(r-r_m)]-2\}$		r_m, ϵ, β
MSV	$V(r)=\begin{cases}\epsilon\exp[-\beta r_m^{-1}(r-r_m)]\{\exp[-\beta r_m^{-1}(r-r_m)]-2\} & r\le r_1 \\ (r_2-r)[S_1(r_2-r)^2+S_3]+(r-r_1)[S_2(r-r_1)^2+S_4] & r_1<r<r_2 \\ -\frac{C_6}{r^6}-\frac{C_8}{r^8} & r>r_2\end{cases}$		r_m, ϵ, β; S_{1-4} fixed by smoothness; C_6, C_8 are fixed (Table III)

origin of the middle potential V_c. The origins of the two end potentials $V_e(x_1)$ and $V_e(x_2)$ are located at $-z/2$ and $+z/2$, respectively; z is the overall molecular length. Because of the symmetry of the molecules, the end potentials are constrained to be identical, even for N_2O.

Unlike the Legendre potentials of Eq. (12), we allowed the $V_c(r)$ and $V_e(x)$ radial potentials to have different mathematical forms; again the r_m and ϵ parameters were varied independently. In addition, these potentials were often fit with two distinct shape parameters, one for $V_c(r)$ and a second for both $V_e(x_1)$ and $V_e(x_2)$.

3. Parameter expansion potentials

For a final mathematical form the anisotropy was introduced into the potential indirectly, by making a few of the potential parameters depend upon γ. A convenient and physically reasonable parameter expansion potential has already been proposed for the $He+CO_2$ potential.[5] This potential consists of an elliptical parametrization for r_m and a Legendre parametrization for ϵ,

$$r_m(\gamma)=r_{m_\perp}\left(\frac{1+r_q\sin^2\gamma}{1+r_q}\right)^{1/2};\quad \epsilon(\gamma)=\epsilon_0+\epsilon_2P_2(\cos\gamma)\,, \tag{14}$$

where, for arbitrary γ, $r_m(\gamma)$ is the value of r at the potential minimum, and $-\epsilon(\gamma)$ is the corresponding potential energy. These angularly dependent $r_m(\gamma)$ and $\epsilon(\gamma)$ are used to construct radial potentials for any γ by using central-field-type potentials,

$$V(r,\gamma)=\epsilon(\gamma)\cdot f[\rho(r,\gamma)];\quad \rho(r,\gamma)=[r/r_m(\gamma)]\,. \tag{15}$$

Since ρ depends on both r and γ, it is not possible to factorize the radial and angular dependences, and hence Legendre terms of all orders are implicitly included in this radial anisotropy parametrization $r_m(\gamma)$.[9] A Legendre parametrization for $r_m(\gamma)$ was also used,

$$r_m(\gamma)=r_{m_0}+r_{m_2}P_2(\cos\gamma)\,, \tag{16}$$

in place of the elliptical $r_m(\gamma)$ of Eq. (14).[9] In some fits, the shape parameter of the interaction potential $f[\rho(r,\gamma)]$ was similarly expanded.

In Table II we present several parametrizations used to construct the anisotropic potential models of Eqs. (12)–(16).[48] Of the parameter expansion potentials [Eqs. (14)–(16)], only the MSV and HFD potential forms have the correct long-range behavior, thus allowing their C_6 and C_8 multipolar expansion coefficients to reproduce the known long-range potentials[49] (for the LJ8 form, C_8 is determined by the other parameters). The same may be assured for the multicenter potentials [Eq. (13)] having an MSV (HFD) central potential V_c with MSV, HFD (with vanishing long-range potentials), or Morse end potentials V_e. We note that if the HFD potential is located on one of the end atoms, the long range C_6 and C_8 coefficients are constrained to be zero and the HFD potential reduces to a single exponential. In all these cases, the MSV or HFD central potential V_c is made to have the correct angularly dependent long-range potential. The long-range coefficients, derived from independent experimental data,[49] are listed in Table III for $He+CO_2$, N_2O, and C_2N_2, and were used in all cases where it was possible to assure the correct long-range behavior. The lengths of these molecules, denoted as z for the multicenter potentials [Eq. (13)], are also given in that table.

Using the anisotropic potential models described above,[52] we calculated IOSA DCS's in the center-of-

TABLE III. Molecular lengths and van der Waals asymptotic dispersion constants.[a]

	$He+CO_2$	$He+N_2O$	$He+C_2N_2$
Molecular length/Å	2.32	2.31	3.70
$C_6(0)/(eV\,Å^6)$	9.98	11.33	18.92
$C_6(2)/(eV\,Å^6)$	2.31	2.62	4.42
$C_8(0)/(eV\,Å^8)$	46.4	52.5	88.0
$C_8(2)/(eV\,Å^8)$	48.4	54.9	94.4

[a]See Ref. 49.

TABLE IV. Central-field intermolecular potentials fit to the experimental DCS.

System[a]	Potential type[b]	r_m/Å	σ/Å	ϵ/meV	Shape parameters[b]	χ^2 [c,d]	$\Delta\alpha/\alpha$ (%)[d]
$He+CO_2$ (41)	SPFD	3.58	3.26	4.51	$b_0=60.7$; $b_1=-6.57$; $c_6=0.89$	2100 (5)	2.79
(18)	SPFD	3.73	3.24	3.33	$b_0=28.6$; $c_6=1.14$	3300 (4)	1.02
$He+N_2O$ (40)	SPFD	3.70	3.34	4.23	$b_0=49.1$; $b_1=5.73$; $c_6=0.81$	2300 (5)	3.01
(17)	SPFD	3.32	2.94	3.81	$b_0=39.1$; $c_6=2.69$	400 (4)	0.41
$He+C_2N_2$ (41)	SPFD	3.79	3.33	3.77	$b_0=31.9$; $b_1=-3.94$; $c_6=1.06$	1900 (5)	2.68
(18)	SPFD	3.24	2.89	3.39	$b_0=42.5$; $c_6=4.25$	2200 (4)	0.83

[a]Experimental conditions given in Table I; the number of experimental data points is given in parentheses. For each system, the first row gives a five-parameter fit to the entire DCS (between $\sim 2°$ and 20°); the second row gives a four-parameter fit to just the low-angle portion of the DCS (between $\sim 2°$ and 6°).

[b]Discussed in Sec. III and Ref. 42. See also Eq. (11).

[c]Scattering intensity normalized to 500 at $\theta=4.8°$; the number of parameters varied is given in parentheses.

[d]Goodness-of-fit statistical indices; discussed in Sec. III and in Ref. 42. Note that despite the large χ^2 statistical indices, $\Delta\alpha/\alpha$ indicates that the fits to the low-angle DCS's are quite good. This is due to the larger absolute (but same relative) weights required for normalized weights to be obtained for the low-angle data. The $\Delta\alpha/\alpha$ statistical index is more appropriate for judging the goodness-of-fit than is the χ^2 one.

mass coordinate frame by evaluating Eq. (9) using a 12-point Gauss–Legendre quadrature. Since the potential (and hence the scattering) is symmetric about $\gamma=\pi/2$, this actually requires calculations at only six values of γ. These results differed insignificantly from a 24-point Gauss–Legendre quadrature. The IOSA DCS's were then averaged extensively over both beams' angular and velocity spreads, identically as in the central-field calculations (Sec. III).

V. RESULTS AND DISCUSSION

A. The central-field assumption

The first question to be addressed is the validity of the usual assumption that central-field fits to molecular scattering data yield the spherically symmetric (orientation averaged) component of the intermolecular potential.[2(b),11,12] For weakly anisotropic interactions in highly quantum systems, this central-field assumption has quantitatively been shown to be valid,[4(a),21(a),53] although use of an anisotropic potential parametrization may yield a better description of the data.[14] In contrast, however, preliminary work on $He+CO_2$ showed that the central-field assumption breaks down for this highly anisotropic interaction.[5]

Interpretations of scattering results for anisotropic interactions have been based for some time on semiclassical calculations.[8] These have shown that the effect of anisotropic potential scattering on integral elastic cross sections is primarily to dampen, or quench, the glory undulations. Similar results were obtained for the supernumary rainbow and rapid quantum oscillatory structure of elastic DCS's. On this basis, "total" (elastic plus inelastic) DCS's not exhibiting the quenching effect, relative to corresponding DCS's from spherically symmetric potentials, have usually been interpreted as being sensitive only to the spherical average of the intermolecular potential.[2,11,12] Such a straightforward application of the semiclassical theory for DCS's may, however, be inappropriate for the highly quantum systems under discussion here.[4(a)] More recently, quantum mechanical calculations have been performed for scattering from anisotropic potentials;[7,14,21(a),54] due to the complexity of this scattering problem, it has usually been necessary to employ approximation techniques.[20] The IOSA has been used, with reasonable potentials,[55] to predict quenching in the DCS of both highly quantum and semiclassical systems.[6,9] It has been shown in Sec. II that the conditions of validity of this approximation are satisfied by the systems under consideration in this paper. Consequently, the IOSA is preferred over the semiclassical theory for interpreting quenching of the DCS oscillations.[9]

By comparing the experimental DCS's and the central-field fitted ones of Fig. 1, it is quite evident that the $He+CO_2$, N_2O, and C_2N_2 scattering patterns exhibit significantly quenched oscillatory structure. Central-field SPFD potential parameters are presented in Table IV for fits to the entire DCS's, and to just the low scattering angle measurements ($\theta \lesssim 6°$). Classically, the latter measurements should be due primarily to long-range interactions, which are more nearly isotropic than are short-range ones. Consequently, it is possible that the central-field assumption may be more appropriate for low-angle DCS's than for ones including scattering at relatively wide angles.

We see from Table IV and Fig. 1 that the central-field SPFD potentials, when fit to the entire measured DCS, provide a poor description of the experimental results. Use of the M^2SV, MSV, or HFD central-field parametrizations do not improve the quality-of-fit. Even the most flexible of the central-field parametrizations fail completely in reproducing the observed quenching of the DCS oscillations. From Fig. 2, it is also evident that inclusion of DCS data other than forward-scattering (i.e., for $\theta \gtrsim 6°$) substantially alters the fitted central-field potentials. This clearly is inconsistent with the central-field assumption, and provides another clear indication that anisotropic effects are important for these systems.

B. Anisotropic potentials for $He+CO_2$

We first present anisotropic potentials fit to the $He+CO_2$ total DCS data because the potential for this sys-

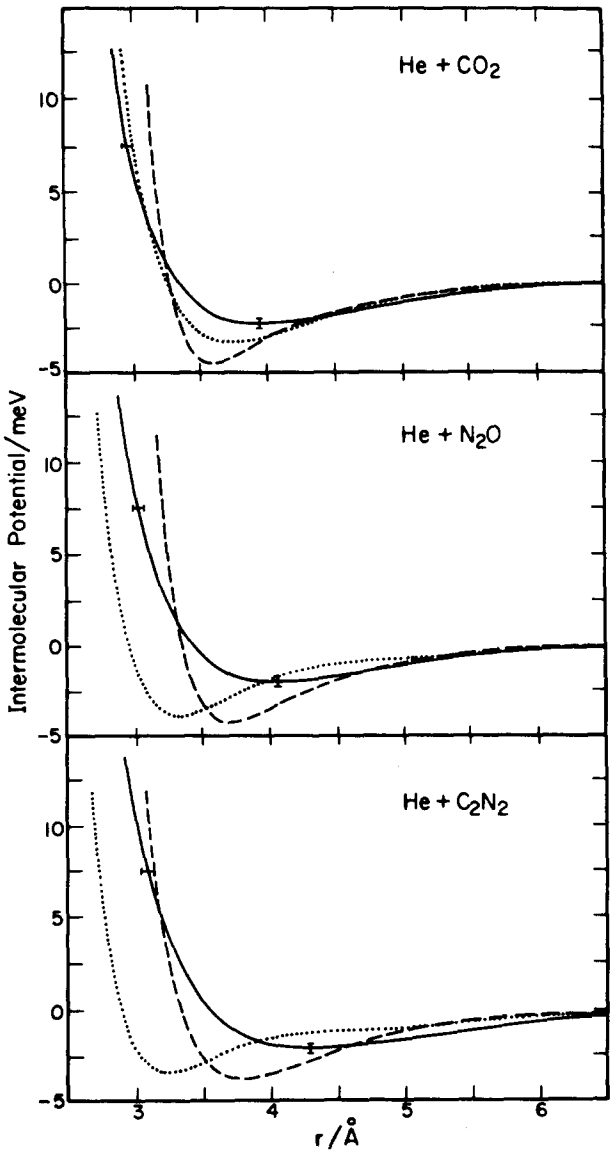

FIG. 2. Spherically symmetric intermolecular potentials for $He+CO_2$, N_2O, and C_2N_2 as functions of the intermolecular separation r. Solid curves: spherical averages of the anisotropic MSV parameter expansion potentials of Eqs. (14)–(16); dashed curves: central-field SPFD potentials; dotted curves: central-field SPFD potentials fit to only the low-angle DCS data ($\theta < 6°$). The error bars on the spherically averaged potentials indicate the accuracy with which isotropic potentials have been determined from DCS data (Ref. 42). Potential parameters are given in Tables III, IV, VIII, and X.

tem has been the subject of various theoretical[55] and experimental[12,56–59] studies. The former have provided reasonable potentials for short- and long-range interactions, while the latter can provide useful constraints on empirical potentials.

The potentials described in Sec. IV B were used to fit the total DCS data for $He+CO_2$. The entire collection of potentials was used in an effort to determine those which could most adequately represent the anisotropy of the interaction.[45] The potentials yielding the best fits to the data can then be compared; their consistency provides some measure of the sensitivity with which different regions of the potential are determined by the present total DCS measurements. It is similarly possible to obtain a reasonable estimate of the accuracy with which different physical parameters are obtainable from the experiment. These parameters may be summarized by considering the potential minimum position and depth for the $\gamma = \pi/2$ configuration ($r_{m_\perp}$ and $\epsilon_\perp$), and for the $\gamma = 0, \pi$ configurations ($r_{m_\parallel}$ and $\epsilon_\parallel$). In addition, we also consider the corresponding values of the spherical average of the anisotropic potentials. These are obtained by expanding the fitted anisotropic potentials in the Legendre series of Eq. (12); the $V_0(r)$ potential minimum position and depth are denoted $r_m(V_0)$ and $\epsilon(V_0)$ respectively. We note that the $r_m(V_0)$ and $\epsilon(V_0)$ are not fitted parameters. Distinct from them are the spherical averaged values of the r_m and ϵ parameters; the latter are denoted r_{m_0} and ϵ_0 and may be fitted parameters [e.g., Eqs. (14) and (16)]. Re-iterating, $r_m(V_0)$ and $\epsilon(V_0)$ are the potential minimum values corresponding to the spherically averaged *potential*, whereas r_{m_0} and ϵ_0 are the spherically averaged potential minimum *parameters*.

Potential parameters and the $\Delta\alpha/\alpha$ goodness-of-fit statistical index for some Legendre expansion potentials [Eq. (12)] are listed in Table V. All of these provide better fits than do the $He+CO_2$ central-field potentials listed in Table IV, and some adequately reproduce the experimental DCS. However, all the Legendre expansion potentials studied exhibit multiple minima in parameter space and high parameter correlations. We have found these potentials to be too unwieldy for practical use, and therefore we exclude them from further discussion.

The results of fitting the multicenter potentials [Eq. (13)] are sampled by Table VI. From this table, and the

TABLE V. Legendre expansion potentials for $He+CO_2$.[a]

Potential type	$\Delta\alpha/\alpha$ (%)[b,c]	$\gamma=\pi/2$		$\gamma=0,\ \pi$		Spherical average	
		$r_{m_\perp}$/Å	$\epsilon_\perp$/meV	$r_{m_\parallel}$/Å	$\epsilon_\parallel$/meV	$r_m(V_0)$/Å	$\epsilon(V_0)$/meV
LJ	2.32(4)	3.16	6.61	4.08	1.51	3.62	2.97
LJ8	2.30(5)	3.16	6.69	4.06	1.64	3.62	3.05
Morse	1.09(5)	3.19	5.07	4.11	3.81	3.78	2.98
MSV	1.12(5)	3.09	4.99	4.04	3.80	3.72	2.82

[a]Discussed in Sec. IV B 1; see Eq. (12).
[b]Goodness-of-fit statistical index; discussed in Sec. III and in Ref. 42.
[c]Number of fitted parameters is in parentheses.

TABLE VI. Multicenter potentials for $He+CO_2$.[a]

Potential type			$\gamma=\pi/2$		$\gamma=0,\ \pi$		Spherical average	
center	end	$\Delta\alpha/\alpha$(%)[b]	$r_{m\perp}$/Å	$\epsilon_\perp$/meV	$r_{m\parallel}$/Å	$\epsilon_\parallel$/meV	$r_m(V_0)$/Å	$\epsilon(V_0)$/meV
LJ8	LJ	2.24(5)	3.30	3.20	4.05	4.12	3.75	3.10
MSV	LJ	1.50(5)	3.50	3.16	4.44	1.81	4.09	2.41
LJ8	HFD	2.23(5)	3.36	5.52	4.52	0.87	3.66	2.92
MSV	HFD	1.50(5)	3.49	3.18	4.43	1.76	4.06	2.41
LJ8	LJ8	1.96(5)	2.93	3.51	4.10	4.30	3.80	3.19
MSV	LJ8	1.52(6)	3.51	3.08	4.46	1.82	4.11	2.39
LJ8	Morse	0.87(6)	3.33	4.08	4.49	2.90	4.05	2.59
Morse[c]	Morse	0.93(5)	3.35	4.16	4.51	2.64	4.05	2.57
MSV	Morse	1.77(5)	3.40	4.90	4.62	1.35	3.85	2.57
LJ8	MSV	0.96(6)	3.39	4.23	4.77	1.42	4.07	2.16
Morse[c]	MSV	1.15(5)	3.46	4.49	4.93	1.06	4.14	2.09
MSV[c]	MSV	0.80(5)	3.38	3.76	4.66	2.03	4.00	2.30

[a]Discussed in Sec. IV B 2; see Eq. (13). z is fixed at 2.32 Å.
[b]See footnote b, Table V.
[c]"Best potentials"—potential parameters are given in Table VIII.

many other fits not summarized there, it can be seen that the end-atom potential types affect the quality-of-fit more than do the central-atom potential types: those potentials with LJ, HFD, or LJ8 potentials on the end atoms result in poorer fits (average $\Delta\alpha/\alpha = 1.8\%$) than those potentials having Morse or MSV end-atom potentials (average $\Delta\alpha/\alpha = 1.1\%$). The best potentials have MSV end-atom potentials, and yield excellent fits to the data (average $\Delta\alpha/\alpha = 1.0\%$).

Finally, in Table VII we present results from fitting the parameter expansion potentials Eqs. [(14)–(16)]. We see that the LJ, HFD, and LJ8 parametrizations are unable to reproduce the measured DCS (average $\Delta\alpha/\alpha = 2.3\%$). In contrast, the Morse and MSV parameter expansion potentials reproduce the measured DCS very well (average $\Delta\alpha/\alpha = 0.8\%$).

Among the anisotropic potentials of Tables VI and VII, those with good fits to the data ($\Delta\alpha/\alpha < 1.5\%$) yield spherically averaged potentials whose minimum positions are all near 4.0 Å, and whose well depths are all near 2.3 meV. It must be noted that these $r_m(V_0)$ and $\epsilon(V_0)$ values are substantially different from the r_m and ϵ parameters obtained by fitting central-field potentials to the DCS data (3.6 Å and 4.5 meV, respectively; cf. Table IV). The differences are 10% for r_m and 90% for ϵ, and may be contrasted with the ±2% and ±10% precision obtained in our previous central-field scattering experiments.[3] Referring again to Fig. 2, it is further apparent that the central-field analyses of the present DCS's do *not* yield the orientation average of the (actual) anisotropic intermolecular potential, even when only low-angle scattering is considered. The central-field assumption is thus *invalid* for the highly anisotropic interactions being considered herein.

Abandoning the central-field assumption, we appraise the results presented in Tables V–VII, for a wide variety of anisotropic parametrizations, evaluating the uniqueness and reliability of the fitted intermolecular potentials. The Legendre expansion potentials [Eq. (12) and Table V] are unreliable, exhibiting large parameter correlations and local minima in the least-squares fitting procedure. This is most likely due to the inadequacy of just a two-term Legendre expansion for the potential (see below). It is apparent that a large number of parameters alone is insufficient to ensure reliable and accurate potentials. Conversely, the multicenter

TABLE VII. Parameter expansion potentials for $He+CO_2$.[a]

Potential type	$\Delta\alpha/\alpha$ (%)[b]	$\gamma=\pi/2$		$\gamma=0,\ \pi$		Spherical average	
		$r_{m\perp}$/Å	$\epsilon_\perp$/meV	$r_{m\parallel}$/Å	$\epsilon_\parallel$/meV	$r_m(V_0)$/Å	$\epsilon(V_0)$/meV
LJ	2.36(4)	3.23	5.30	4.33	3.49	3.63	2.83
HFD	2.49(5)	3.32	4.94	4.67	1.32	3.86	2.54
LJ8	2.07(5)	3.18	5.73	4.04	2.85	3.63	3.21
Morse[c]	0.68(5)	3.30	3.85	4.57	3.29	3.98	2.58
MSV–[c] elliptical	0.82(5)	3.31	3.94	4.77	1.14	3.93	2.35
MSV[c]	0.83(5)	3.33	3.83	4.88	1.19	3.97	2.34

[a]Discussed in Sec. IV B 3; see Eqs. (14)–(16).
[b]See footnote b, Table V.
[c]Best potentials—potential parameters are given in Table VIII.

TABLE VIII. Parameters for best He + CO_2 potentials.

Potential type center[a]	end[a]	$\Delta\alpha/\alpha$ (%)	r_{m_α}/Å	ϵ_α/meV	r_{m_β}/Å	ϵ_β/meV	Shape parameter	$\gamma=\pi/2$ $r_{m_\perp}$/Å	$\gamma=\pi/2$ $\epsilon_\perp$/meV	$\gamma=0,\pi$ $r_{m_\parallel}$/Å	$\gamma=0,\pi$ $\epsilon_\parallel$/meV	Spherical average $r_m(V_0)$/Å	Spherical average $\epsilon(V_0)$/meV
Morse	Morse	0.93	3.98	0.30	3.38	2.28	5.12	3.35	4.16	4.51	2.64	4.05	2.57
Morse	MSV	1.15	3.16	4.82	4.20	0.51	4.64	3.46	4.49	4.93	1.06	4.14	2.09
MSV	MSV	0.80	3.65	0.57	3.49	1.65	4.39	3.38	3.76	4.66	2.03	4.00	2.30
EG(MSV + MSV)[a,d]		1.20	3.93	0.64	3.57	1.64	4.65	3.55	3.61	4.70	2.02	4.15	2.33
Morse[b]		0.68	3.72	3.66	0.85	−0.37	5.68	3.30	3.85	4.57	3.29	3.98	2.58
MSV-elliptical[c]		0.82	3.31	2.95	−0.52	−1.91	4.59	3.31	3.94	4.77	1.14	3.93	2.34
MSV[b]		0.83	3.84	1.05	0.99	−0.67	4.59	3.33	3.83	4.88	1.19	3.97	2.22
EGMSV[b,d]		1.30	3.94	1.05	0.90	−0.68	5.00	3.48	4.13	4.84	1.39	4.09	2.29
Average		0.96	...	...	...	...	...	3.40	3.97	4.73	1.85	4.04	2.34
Standard deviation		...	...	...	...	...	...	0.09	0.28	0.15	0.80	0.08	0.17

[a]Multicenter potentials, see Eq. (13). r_{m_α} and ϵ_α are minimum parameters for the central atom; r_{m_β} and ϵ_β are those for the end atoms.

[b]Parameter expansion potentials, see Eqs. (14)–(16). r_{m_α} and r_{m_β} correspond to r_{m_0} and r_{m_2} in Eq. (16); ϵ_α and ϵ_β correspond to ϵ_0 and ϵ_2 in Eq. (14).

[c]Parameter expansion potential, see Eqs. (14) and (15). r_{m_α} and r_{m_β} correspond to $r_{m_\perp}$ and r_e in Eq. (14); ϵ_α and ϵ_β correspond to ϵ_0 and ϵ_2 in Eq. (14).

[d]Electron-gas potential [Ref. 53(a)] has been used for the short-range interaction. See Sec. V D.

potentials [Eq. (13) and Table VI] have smaller parameter correlations, and yield good fits, when the parametrizations for each center are realistic and flexible (especially the MSV form). The same may be said of the parameter expansion potentials [Eqs. (14)–(16) and Table VII].

We collect the "best" potentials in Table VIII. The criteria of good fits to the DCS data, and realistic potentials with statistically significant parameter values, has led to a set of rather similar potentials (especially for the $\gamma=\pi/2$ configuration, see below). These same potential types are used in fitting the He + N_2O and He + C_2N_2 scattering data (Sec. V C below).

Among the potentials of Table VIII, those having the correct long-range behavior (see Table III) are the multicenter MSV + MSV potential, and the MSV parameter expansion potentials. In Sec. V D below, the reliability of two of these potentials will be improved further by considering data more sensitive to the short-range repulsion than are our total DCS measurements. Contour plots of the resulting "EG(MSV + MSV)" and "EGMSV" potentials are shown in Figs. 3 and 4, respectively, and are considered reliably to represent the overall shape of the He + CO_2 anisotropic potential. As we shall see below, the potentials are more reliable around the $\gamma=\pi/2$ configuration than elsewhere. Of course, the relative crudeness of the experiment (e.g., the measurements do not resolve inelastic contributions to the DCS) suggests that these contour plots should be relied on only to give an overall "shape" of the anisotropic He + CO_2 intermolecular potential.

Referring again to Table VIII, we see that the well position is determined with little variation among any of the best potentials, for both the orientation angles

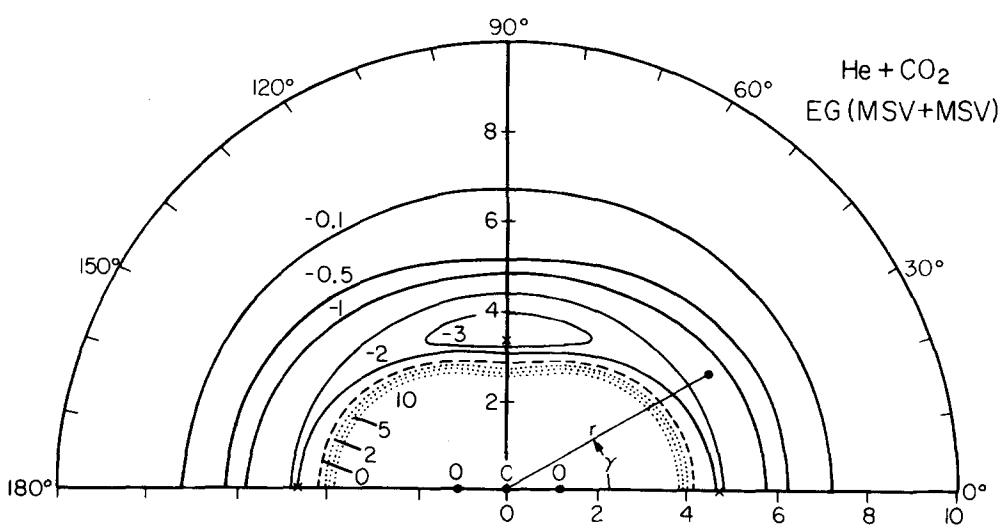

FIG. 3. He + CO_2 empirical potential energy surface, calculated from the anisotropic EG(MSV + MSV) parametrization of Eqs. (13) and (17). Potential energy contours (in meV) are displayed for $V(r,\gamma) \leq 10$ meV; the polar coordinates are r (in Å) and γ. Solid contours: $V(r,\gamma)<0$; dashed contour: $V(r,\gamma)=0$; dotted contours: $V(r,\gamma)>0$. The absolute minimum on the potential surface is −3.61 meV and occurs at $\gamma=\pi/2$, $r=3.55$ Å. Saddle points occur for the collinear configurations $\gamma=0$, π, $r=4.70$ Å, where the potential is −2.02 meV. The absolute minimum and saddle point configurations are denoted by crosses. The positions of the C and O atoms are also shown for reference.

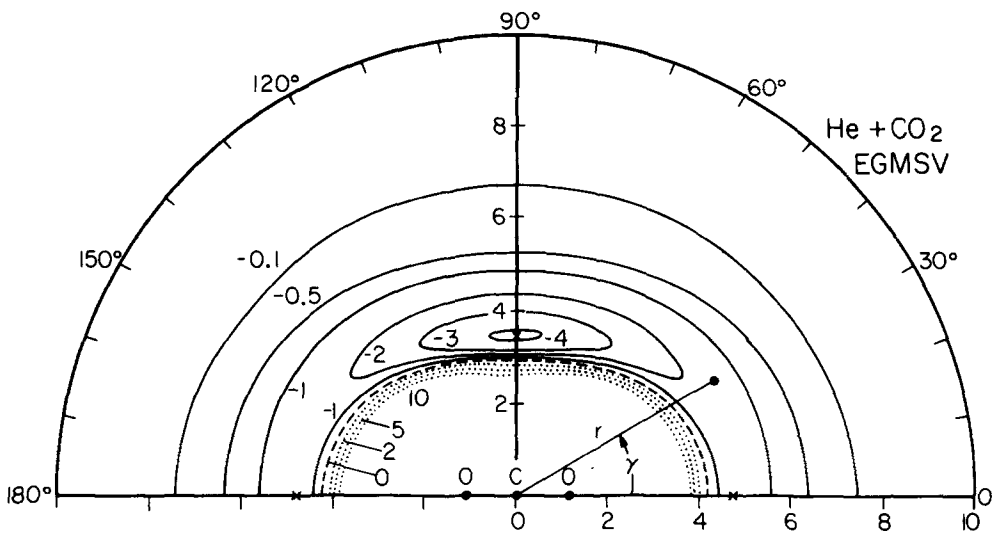

FIG. 4. $He+CO_2$ empirical potential energy surface, calculated from the anisotropic EGMSV parametrization of Eqs. (14)–(17). Symbols as in Fig. 3. The absolute minimum is -4.13 meV, at $\gamma=\pi/2$, $r=3.48$ Å; saddle points occur at $\gamma=0$, π, $r=4.84$ Å, where the potential is -1.39 meV.

$\gamma=0$ and $\gamma=\pi/2$. As expected from the linearity of the CO_2 molecule, we find that $r_{m_\parallel} > r_{m_\perp}$. The relatively greater sensitivity of the DCS data to radial anisotropies than to the well depth anisotropies is analogous to the sensitivity with which r_m and ϵ may be determined from scattering measurements for spherically symmetric, highly quantum, interactions. The well depth is consistent to within $\pm 7\%$ for $\gamma=\pi/2$, a precision approaching that attained in central-field scattering experiments. Although the well depth for $\gamma=0$ is not precisely determined, it is apparent in any case that $\epsilon_\parallel$ is significantly less than $\epsilon_\perp$, implying a T-shaped (C_{2v}) equilibrium configuration for $He+CO_2$. This T-shaped equilibrium configuration has been predicted[55] and found[60] for the similar $Ar+CO_2$ and $Ar+OCS$ systems, respectively. We stress that all the potential parametrizations used in this study are sufficiently flexible to allow fitted potentials to be either linear or T shaped. Almost invariably however, the best-fit potentials have profoundly deeper wells at $\gamma=\pi/2$ than at $\gamma=0$. For example, fitting the DCS with first-guess

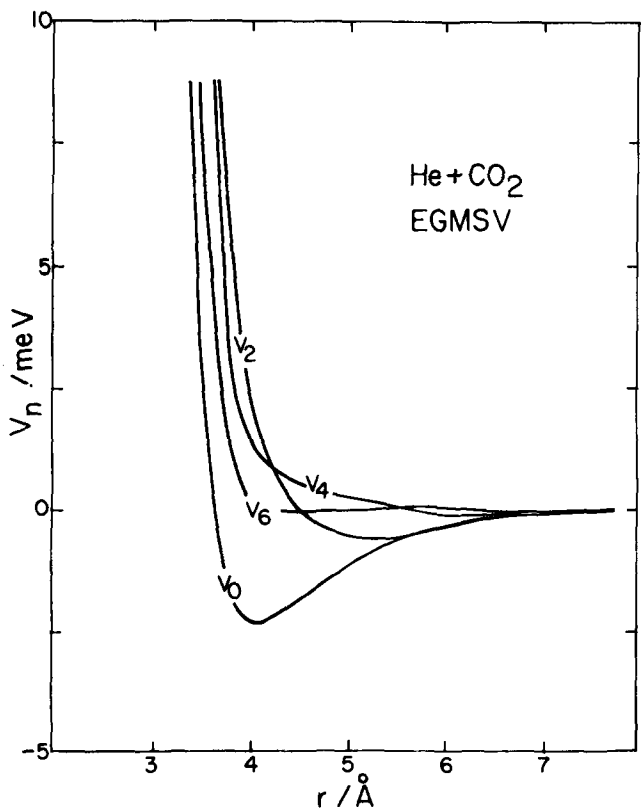

FIG. 5. EGMSV potential for $He+CO_2$, plotted as a function of r, for Legendre expansion coefficients V_0 through V_6.

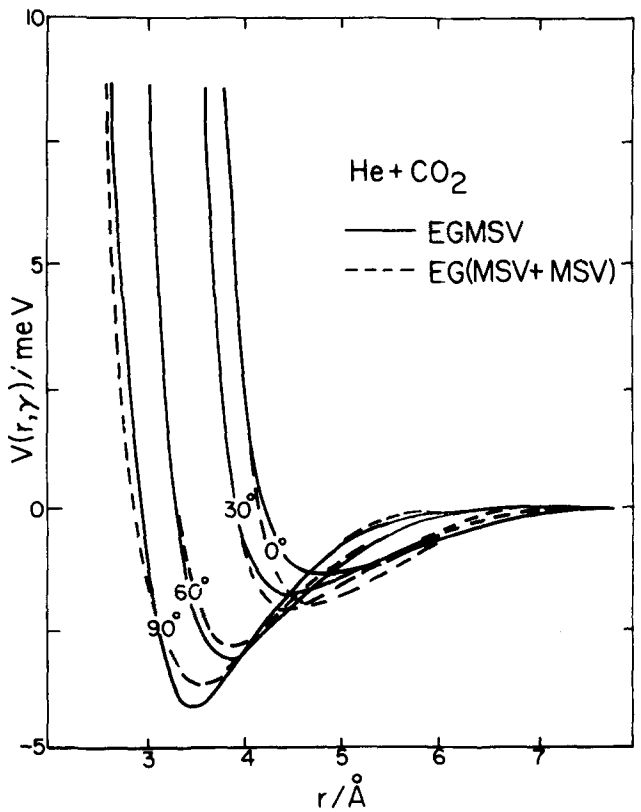

FIG. 6. Anisotropic potentials for $He+CO_2$, plotted as functions of r with fixed orientation angles γ, for γ between 0° and 90°. Solid lines: EGMSV potential; dashed lines: EG(MSV+MSV) potential.

TABLE IX. The effect of neglecting small-angle DCS data for $He+CO_2$.[a]

Smallest angle	$\Delta\alpha/\alpha$ (%)	$\gamma=\pi/2$		$\gamma=0,\ \pi$		Spherical average	
		$r_{m_\perp}$/Å	$\epsilon_\perp$/meV	$r_{m_\parallel}$/Å	$\epsilon_\parallel$/meV	$r_m(V_0)$/Å	$\epsilon(V_0)$/meV
1.60	0.83	3.33	3.83	4.48	1.19	3.97	2.22
2.10	0.69	3.34	3.79	4.91	1.41	4.01	2.21
2.60	0.74	3.34	3.84	4.84	1.49	3.99	2.28
3.10	0.80	3.33	3.93	4.79	1.79	4.00	2.36
4.10	1.09	3.34	3.85	4.89	1.26	3.98	2.25
5.10	1.43	3.34	3.83	4.89	1.28	3.99	2.31

[a]Considering the MSV parameter expansion potential.

parameters corresponding to a linear $He+CO_2$ configuration nevertheless results in a T-shaped best-fit potential.

The EGMSV potential, obtained from fitting the DCS data and shown in Fig. 4, has been expanded in the Legendre series of Eq. (12) for terms up to $n=6$; the radial factors $V_n(r)$ are displayed in Fig. 5. It is immediately seen that even the attractive minimum region has significant components through the $n=4$ term. In Fig. 6, we display the radial potential for cuts along the $\gamma=0°$, 30°, 60°, and 90° orientation angles, for the EGMSV and EG(MSV+MSV) potentials. As indicated by the standard deviations of the $\epsilon_\perp$ and $\epsilon_\parallel$ parameters shown in Table VIII, the consistency between these radial cuts is good for $\gamma=\pi/2$, becoming progressively worse as γ is decreased towards 0. The fact that $r_{m_\perp}$ is determined more accurately that $r_{m_\parallel}$, and $\epsilon_\perp$ more accurately than $\epsilon_\parallel$, can be interpreted as due to the configuration space being larger for near-perpendicular approaches than for near-collinear ones.

To ensure that the above conclusions are free of systematic errors possibly introduced by considering low-angle scattering data,[2(d)] we show in Table IX the effect of neglecting such data. It is clear that the potential minimum parameters, and in particular the well depths, are unaffected by including or excluding the low-angle DCS measurements. Only the quality-of-fit is reduced by restricting the number of data points.

C. Anisotropic potentials for $He+N_2O$ and $He+C_2N_2$

The DCS's for these systems, shown in Fig. 1, were fit by the (five-parameter) potential parametrizations that proved most successful in the analysis of $He+CO_2$ scattering presented above. The results of this fitting, including potential minimum parameters, are shown in Table X. The $He+N_2O$ DCS data are accurately reproduced. For $He+C_2N_2$, the multicenter MSV+MSV parametrization and the elliptical MSV parameter expansion potentials fail to accurately reproduce the DCS data. The most convenient and reliable of the best potentials is the parameter expansion MSV potential. Contour plots for $He+N_2O$ and $He+C_2N_2$ for this parametrization are presented in Figs. 7 and 8, respectively. In Figs. 9 and 10, we display the radial potential for cuts along the $\gamma=0°$, 30°, 60°, and 90° orientation angles for the $He+N_2O$ and $He+C_2N_2$ potentials, re-

TABLE X. Parameters for best $He+N_2O$ and $He+C_2N_2$ potentials.

Potential type								$\gamma=\pi/2$		$\gamma=0,\ \pi$		Spherical average	
center[a]	end[a]	$\Delta\alpha/\alpha$ (%)	r_{m_α}/Å	ϵ_α/meV	r_{m_β}/Å	ϵ_β/meV	Shape parameter	$r_{m_\perp}$/Å	$\epsilon_\perp$/meV	$r_{m_\parallel}$/Å	$\epsilon_\parallel$/meV	$r_m(V_0)$/Å	$\epsilon(V_0)$/meV
$He+N_2O$													
Morse	Morse	1.01	5.11	0.04	3.38	2.86	5.38	3.35	4.25	4.53	3.02	4.11	2.61
Morse	MSV	1.36	5.14	5.45	4.83	0.56	4.25	3.50	4.71	5.03	1.04	4.25	2.00
MSV	MSV	1.42	2.92	2.60	3.62	0.94	5.62	3.23	3.73	4.57	2.88	4.30	2.49
Morse[b]		0.83	3.77	3.80	0.92	−0.48	5.94	3.31	4.03	4.69	3.33	4.08	2.48
MSV-elliptical[c]		0.95	3.35	2.95	−0.56	−2.49	4.40	3.35	4.20	5.05	0.46	4.40	2.03
MSV[b]		1.06	3.98	1.00	1.17	−0.88	4.53	3.39	4.22	5.14	1.13	4.09	2.08
Average		1.11	...	...	...	...	...	3.36	4.19	4.84	1.98	4.21	2.28
Standard deviation		...	...	...	...	...	...	0.09	0.32	0.27	1.24	0.13	0.27
$He+C_2N_2$													
Morse	Morse	1.29	4.08	0.82	3.22	2.85	5.21	3.61	2.82	5.04	3.27	4.54	2.16
Morse	MSV	1.19	3.88	1.62	3.63	1.20	4.23	3.66	3.48	5.34	1.76	4.56	1.85
MSV	MSV	2.07	4.11	0.98	3.61	1.48	3.82	3.70	3.13	5.40	2.04	4.59	1.86
Morse[b]		1.37	3.90	3.76	0.88	−0.26	5.73	3.46	3.89	4.78	3.52	4.17	2.65
MSV-elliptical[c]		1.75	3.52	2.76	−0.61	−2.65	4.05	3.52	4.09	5.63	0.11	4.29	2.08
MSV[b]		1.19	4.26	0.71	1.33	−2.27	3.80	3.60	4.55	5.59	0.41	4.13	2.06
Average			...	...	...	...	...	3.59	3.66	5.30	1.85	4.38	2.11
Standard deviation		...	...	...	...	...	...	0.09	0.64	0.33	1.41	0.21	0.29

[a]See note (a) of Table VIII. [b]See note (b) of Table VIII. [c]See note (c) of Table VIII.

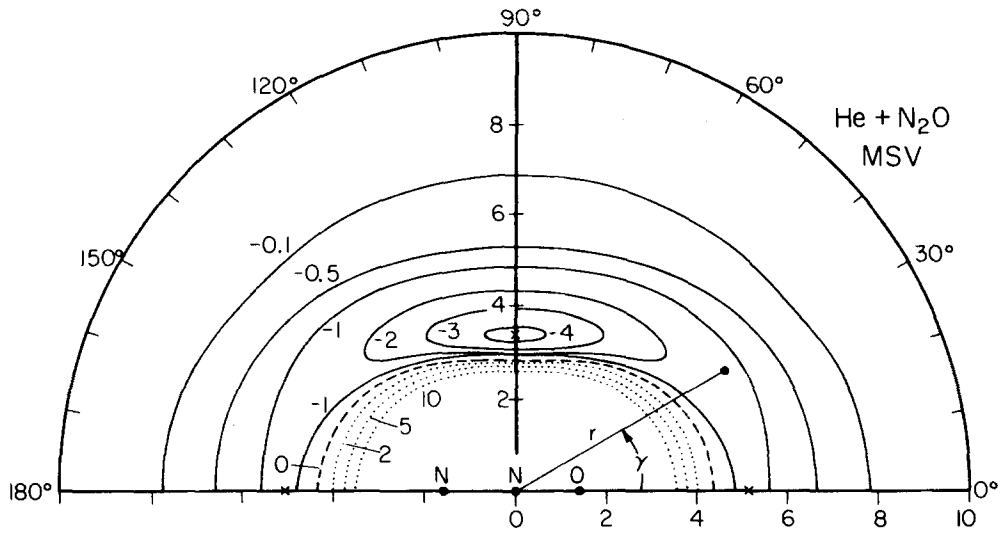

FIG. 7. He+N_2O empirical potential energy surface, calculated from the MSV parameter expansion potential of Eqs. (14)–(16). Symbols as in Fig. 3. The absolute minimum is −4.22 meV at $\gamma=\pi/2$, $r=3.39$ Å; saddle points occur at $\gamma=0$, π, $r=5.14$ Å, where the potential is −1.13 meV.

spectively. As indicated in Table X, and by the results for He+CO_2, the region of the potential surface determined most reliably is in the vicinity of the perpendicular configuration. Since only the total DCS data were available for obtaining the He+N_2O and He+C_2N_2 anisotropic potentials, we consider them to be less reliable than the He+CO_2 EGMSV potential (see Sec. V D).

In Table XI, we compare potential minimum parameters for He+N_2O and He+C_2N_2 with those for He+CO_2. The only significant trend observed is that He+C_2N_2 has larger radial minima ($r_{m_\perp}$, $r_{m_\parallel}$ and $r_m(V_0)$) than either He+CO_2 or He+N_2O. This may be expected from the lengths of these molecules. More surprisingly, it seems that the well depth anisotropy is less for He+C_2N_2 than for He+CO_2 and He+N_2O, though all three systems have absolute potential minima in the perpendicular configuration.

D. Short-range He+CO_2 potential and comparison with experiment

We have extended the He+CO_2 MSV+MSV multicenter potential and the MSV parameter expansion potential to short radial distances, obtaining what we term the EG(MSV+MSV) and EGMSV potentials, respectively. This may be accomplished by using the electron-gas potential[55(a)] at short distances, and then smoothly joining on to the MSV+MSV multicenter potential, or to the MSV parameter expansion potential, at larger distances. The DCS's are largely insensitive to these changes. The interaction potentials are given by

$$V(r,\gamma)=V_{EG}(r,\gamma)\exp\left\{-\left[\frac{0.75r_m(\gamma)}{r}\right]^{15}\right\}+V_p(r,\gamma)\left(1-\exp\left\{-\left[\frac{0.75r_m(\gamma)}{r}\right]^{15}\right\}\right), \quad (17)$$

p = MSV or MSV+MSV .

The parameters 0.75 and 15 were chosen by requiring that $V(r,\gamma)$ is 37% V_p at $r=0.75r_m(\gamma)$ and that $V(r,\gamma)$ is 99% V_p at $r=r_m(\gamma)$. No attempt was made to vary these parameters. For the EGMSV potential, $r_m(\gamma)$ is given by Eq. (16); for the EG(MSV+MSV) potential, $r_m(\gamma)$ is found from Eq. (13). The fitted EGMSV and EG(MSV+MSV) potential parameters and $\Delta\alpha/\alpha$ goodness-of-fit statistical index are given in Table VIII. This extension

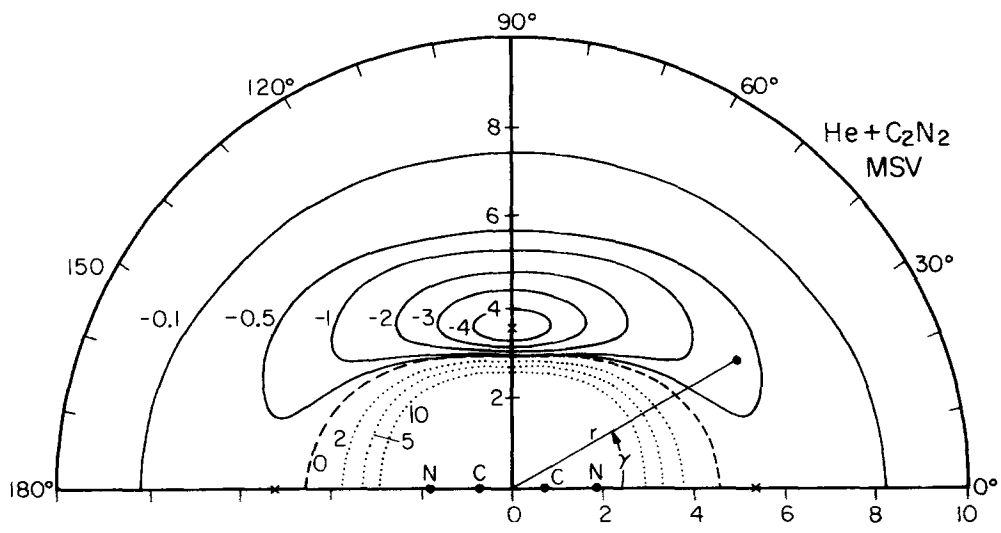

FIG. 8. He+C_2N_2 empirical potential energy surface, calculated from the MSV parameter expansion potential of Eqs. (14)–(16). Symbols as in Fig. Fig. 3. The absolute minimum is −4.55 meV at $\gamma=\pi/2$, $r=3.60$ Å; saddle points occur at $\gamma=0$, π, $r=5.59$ Å, where the potential is −0.41 meV.

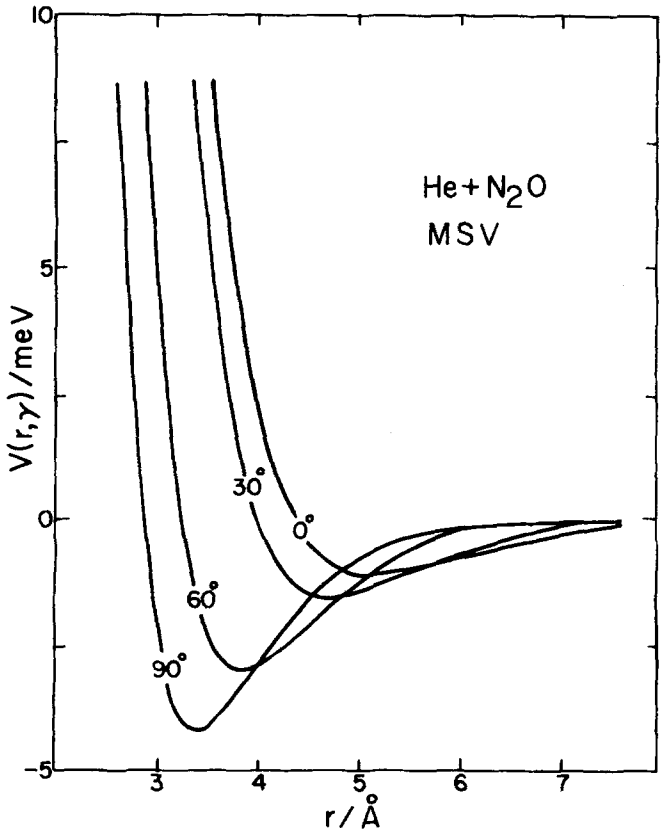

FIG. 9. MSV parameter expansion potential for $He+N_2O$, plotted as a function of r with fixed orientation angles γ, for γ between 0° and 90°.

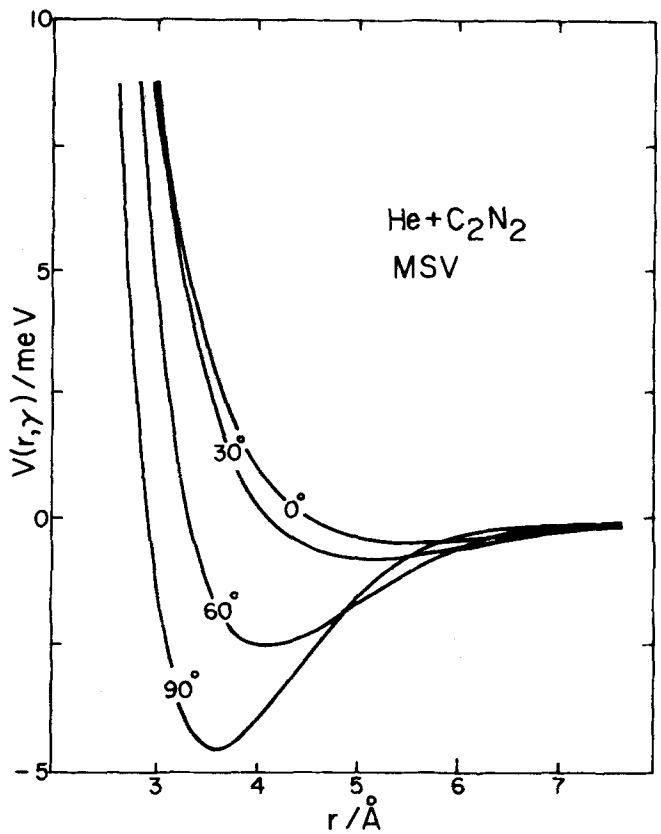

FIG. 10. MSV parameter expansion potential for $He+C_2N_2$, plotted as a function of r with fixed orientation angles γ, for γ between 0° and 90°.

to short radial distances allows a comparison to be made between the potential obtained from Eq. (17) and properties sensitive to the repulsive wall of the potential and its anisotropy.

The classical second virial coefficient for angle-dependent potentials is given by[61]

$$B(T) = \int_0^\infty r^2 dr \int_{-1}^{1} dx \{1 - \exp[-V(r,x)/k_B T]\} , \qquad (18)$$

where $x = \cos\gamma$, k_B is Boltzmann's constant, and T is the temperature. Our calculated second virial coefficients are shown in Fig. 11, where one sees that agreement is acceptable considering the scatter in the experimental results. It should also be noted that we made no attempt to include quantum corrections, which should shift our results upwards. The EG(MSV+MSV) and EGMSV anisotropic potentials produce results so similar that only the EGMSV potential need be considered further. We also see that the spherical average of the anisotropic EGMSV potential predicts second virial coefficients substantially higher than the experimental results.

The viscosity and binary diffusion coefficients are given by[62]

$$\eta = \frac{5k_B T}{8\Omega^{(2,2)}} \qquad (19)$$

and

$$D = \frac{3k_B T}{16 N \mu \Omega^{(1,1)}} , \qquad (20)$$

where μ is the reduced mass and N is the total number density (molecules/cm^3) of the gas. The collision integrals are defined by[6,7,63,64]

TABLE XI. Best potential minimum parameters for $He+CO_2$, $He+N_2O$, and $He+C_2N_2$.

System[a]	$\Delta\alpha/\alpha$ (%)	z/Å	$r_{m_\perp}$/Å	$\epsilon_\perp$/meV	$r_{m_\parallel}$/Å	$\epsilon_\parallel$/meV	$r_m(V_0)$/Å	$\epsilon(V_0)$/meV
$He+CO_2$	0.96	2.32	3.40	3.97	4.73	1.85	4.04	2.34
$He+N_2O$	1.11	2.31	3.36	4.19	4.84	1.98	4.21	2.28
$He+C_2N_2$	1.48	3.70	3.59	3.66	5.30	1.85	4.38	2.11
Precision[b]	...	...	0.1	0.3	0.2	0.8	0.1	0.2

[a]Recommended for use are the MSV parameter expansion potentials (EGMSV for $He+CO_2$).
[b]For $He+CO_2$.

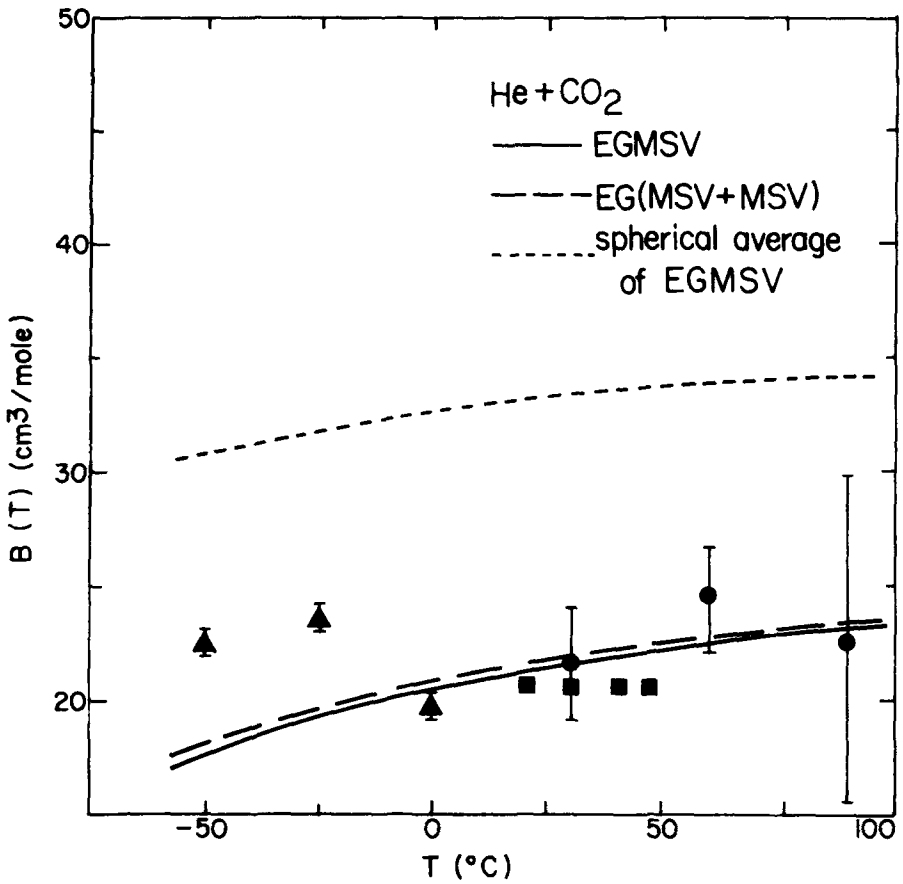

FIG. 11. Comparison of calculated and experimental second virial coefficients B, for $He+CO_2$, as functions of the temperature, T. The triangles are taken from the experiments of Brewer (Ref. 56); circles from Cottrell *et al.* (Ref. 57); and squares from Bell and Dunlop (Ref. 58). The curves are classical virial coefficients calculated from the empirical potentials. Solid curve: anisotropic EGMSV potential; long dashed curve: anisotropic EG(MSV+MSV) potential; short dashed curve: spherical average of the anisotropic EGMSV potential.

$$\Omega^{(n,s)} = \frac{1}{2}\left(\frac{k_B T}{2\pi\mu}\right)^{1/2} \frac{1}{(k_B T)^{s+2}} \int_0^\infty d\xi\, \xi^{s+1} \exp(-\xi/k_B T)\, Q^{(n)}(\xi) , \tag{21}$$

where $Q^n(\xi)$ are the generalized integral cross sections

$$Q^n(\xi) = q_r^{-1} \sum_j (2j+1) \exp(-\xi_j/k_B T) \times \sum_{j'} \int d\mathbf{r}\, I(j' \leftarrow j|\theta)\, \Phi_n(\xi) \tag{22}$$

with

$$\Phi_1(\xi) = 1 - (\xi'/\xi)^{1/2} \cos\theta \tag{23}$$

and

$$\Phi_2(\xi) = 1 - (\xi'/\xi)\cos^2\theta - (1/6)(1-\xi'/\xi)^2 . \tag{24}$$

In these expressions ξ and ξ' are the incident and final relative kinetic energies, $I(j' \leftarrow j|\theta)$ is the degeneracy-averaged DCS, and q_r is the rotational partition function

$$q_r = \sum_j (2j+1) \exp(-\xi_j/k_B T) . \tag{25}$$

Within the IOSA it is easily shown that[6]

$$Q^n(\xi) = \frac{1}{2} \int_{-1}^{1} Q^{(n)}(\xi;\gamma) d\cos\gamma , \tag{26}$$

where

$$Q^{(1)}(\xi;\gamma) = (4\pi/k_i^2) \sum_l (l+1) \sin^2[\eta_{l+1}(\gamma) - \eta_l(\gamma)] \tag{27}$$

and

$$Q^{(2)}(\xi;\gamma) = (4\pi/k_i^2) \sum_l \frac{(l+1)(l+2)}{2l+3} \sin^2[\eta_{l+2}(\gamma) - \eta_l(\gamma)] , \tag{28}$$

where the $\eta_l(\gamma)$ are the phase shifts of Eq. (7). The diffusion coefficients are compared with experiment in Fig. 12, where one sees the agreement is excellent. Also shown are diffusion coefficients from the spherically averaged potential, which fall below the experiment and have the wrong slope. This is consistent with the results from the $He+CO_2$ electron-gas potential.[6]

The viscosity coefficient of a binary mixture is given by[63]

$$\eta_{mix} = [H_{22}X_1^2 - 2H_{12}X_1X_2 + H_{11}X_2^2]/[H_{11}H_{22} - H_{12}^2] , \tag{29}$$

where the X_i are the mole fractions of the two species and

$$H_{11} = \frac{X_1^2}{\eta_1} + \frac{2X_1X_2}{(m_1+m_2)}\left[\frac{1}{ND_{12}} + \frac{m_2\mu_{12}}{m_1\eta_{12}}\right] , \tag{30}$$

$$H_{22} = \frac{X_2^2}{\eta_2} + \frac{2X_1X_2}{(m_1+m_2)}\left[\frac{1}{ND_{12}} + \frac{m_1\mu_{12}}{m_2\eta_{12}}\right] , \tag{31}$$

and

$$H_{12} = -\frac{2X_1X_2}{(m_1+m_2)}\left[\frac{1}{ND_{12}} - \frac{\mu_{12}}{\eta_{12}}\right] . \tag{32}$$

Here m_i are the masses of the two species, μ_{12} their reduced mass, η_i are the viscosity coefficients of the pure components, and η_{12} and D_{12} are the viscosity and

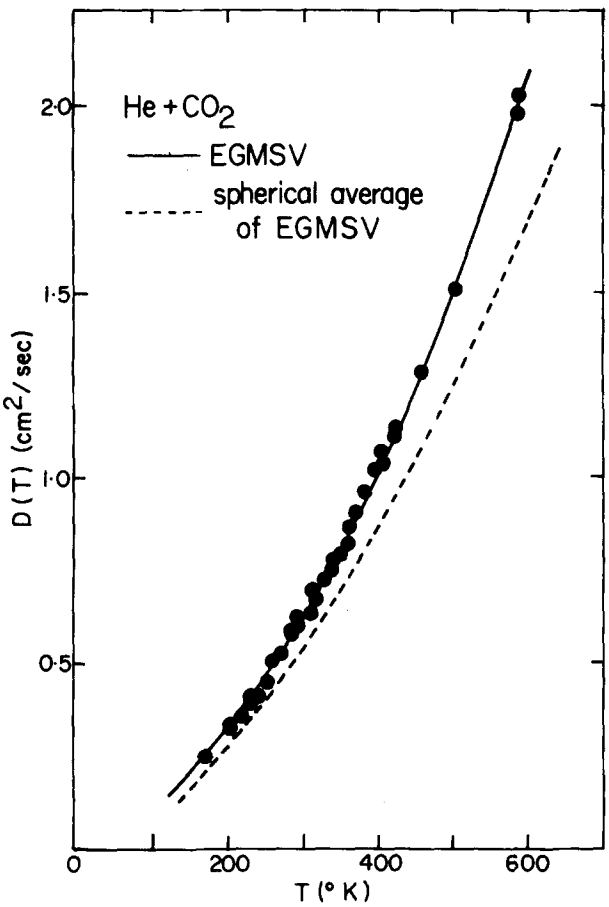

FIG. 12. Comparison of calculated and experimental diffusion coefficients D, for $He+CO_2$, as functions of the absolute temperature T. The points are taken from the experiments of: Loiko *et al.* (Ref. 59); Nagata and Hasegawa (Ref. 63); Ivakin and Suetin (Ref. 65); and Kosov *et al.* (Ref. 66). The curves are calculated from the empirical potentials. Solid curve: anisotropic EGMSV potential; dashed curve: spherical average of the anisotropic EGMSV potential.

diffusion coefficients of Eqs. (19) and (20).

Measurements of the viscosity of $He+CO_2$ mixtures accurate to 0.1% to 0.3% at nine mole fractions and eight temperatures ranging from 20 to 700 °C have been reported by Kestin and Ro.[67] To make comparisons with their results, we did calculations using the experimental η_i of the pure components but the theoretical D_{12} and η_{12}. The results using the anisotropic EGMSV potential and its spherical average are shown in Fig. 13 for the highest and lowest temperatures. Once again, we see that the anisotropic results are in excellent agreement with the experiment, whereas the results from the spherically averaged potential are in very poor agreement with experiment.

The total integral cross section for the scattering of He by CO_2 has been measured by Butz *et al.*[12] The results calculated from our anisotropic potentials, and including velocity averaging, are shown in Fig. 14, where one sees that the agreement is quite good. Again this good agreement is lost when the spherically averaged potential is considered in place of the anisotropic potential. Agreement at the lower end of the velocity range is probably fortuitous, since the IOSA is expected to break down when the most probable relative kinetic energy is not large compared to the rotational energy level spacing.

Consideration of properties other than the DCS measurements obtained in this study show that the anisotropic EGMSV potential for $He+CO_2$ is consistent with reported measurements of virial, diffusion, and viscosity coefficients, as well as integral collision cross sections. This good agreement is lost when the spherical average of the anisotropic potential is used to evaluate these properties instead. This in turn implies that the equilibrium, gas transport properties, and cross sections are sensitive to potential anisotropies, and should not be studied without considering their contributions. While progress towards inversion of such data to yield anisotropic intermolecular potentials is being made,[68] the most productive route probably lies in multiple-property fitting to realistic intermolecular potentials.[45,69] The latter procedure has been found useful in determining atom–atom potentials, even with the availability of highly accurate DCS data.[2]

VI. SUMMARY AND CONCLUSIONS

By measuring the differential cross sections (DCS) for scattering of a room-temperature nozzle beam of He by crossed beams of CO_2, N_2O, and C_2N_2, we have determined physically realistic intermolecular potentials for these systems. These potentials have large anisotropies, both in the well depth and in the position of the attractive minimum. Central-field analyses of the scattering data yield potentials that are *not* the orientation averages of the anisotropic intermolecular potentials.[4] Moreover, even very flexible central-field potential parametrizations are unable to adequately reproduce the measured DCS's. The central-field assumption fails even when only that part of the DCS least sensitive to repulsive interactions is considered in the analysis.

Mathematical forms most suitable for describing the large potential anisotropies of these systems are the parameter expansion potentials and multicenter potentials, incorporating the correct long-range behavior. The most convenient and reliable of these best potentials is the MSV parameter expansion potential [Eqs. (14)–(16)]. Its mathematical form relates clearly the parameter values with features of the intermolecular potential, and it has proven successful in fitting all three systems studied here.

The best-fit potentials to these systems indicate that a T-shaped configuration has roughly twice the stability of a collinear one. As expected from the molecular shape, the attractive minimum position is substantially further from the molecular center-of-mass for the collinear configuration than for the perpendicular configuration.

The repulsive wall for the $He+CO_2$ anisotropic potential, obtained from electron-gas calculations, has been joined to the anisotropic potential obtained from the present scattering data. Equilibrium and gas transport properties have been calculated from the resulting

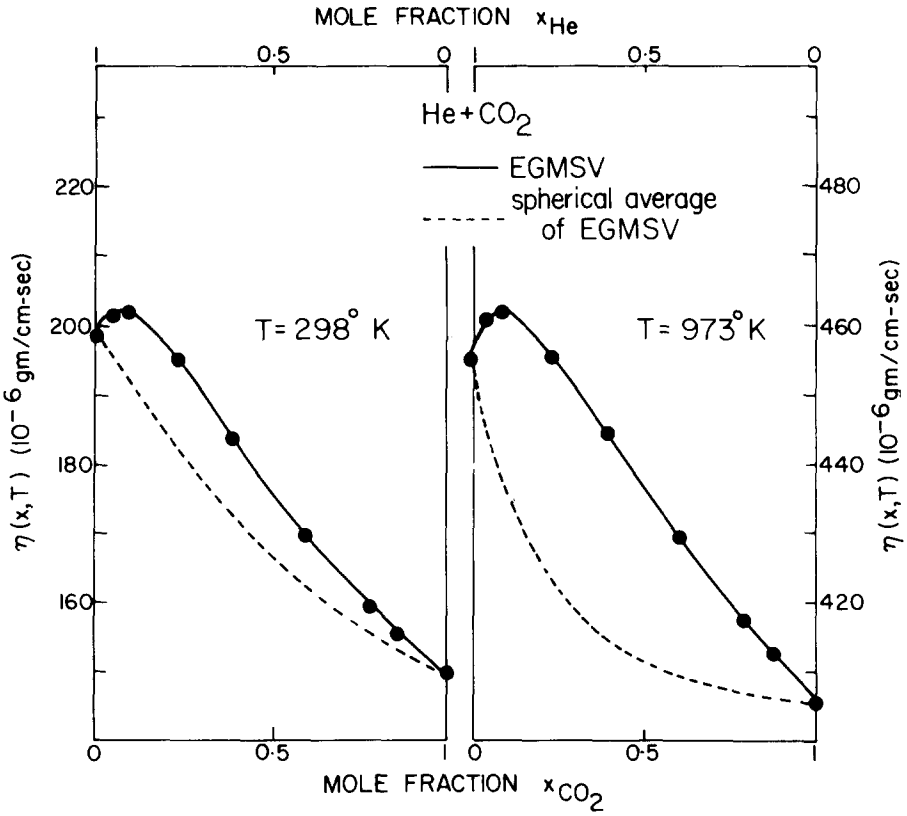

FIG. 13. Comparison of calculated and experimental binary viscosity coefficients η, for $He+CO_2$, as a function of the mole fraction x at $T=298$ and 973 K. The data are taken from the experiments of Kestin and Ro (Ref. 67). The curves are calculated from the empirical potentials as in Fig. 12.

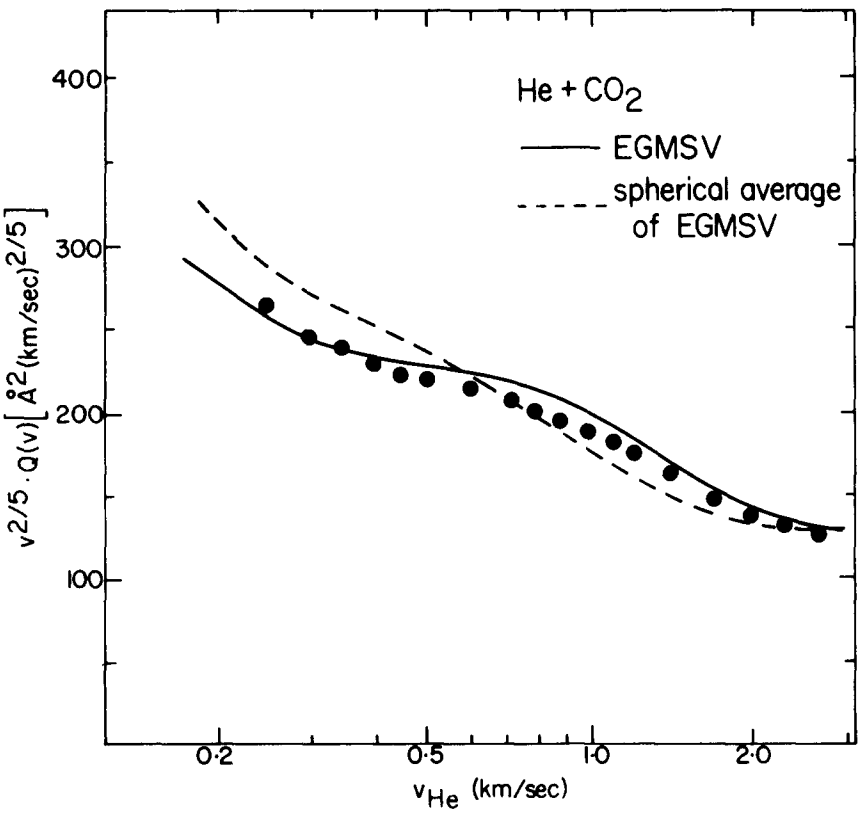

FIG. 14. Comparison of calculated and experimental total integral cross sections Q, for $He+CO_2$, as a function of the He beam velocity v_{He}. The data are experimental results of Butz *et al.* (Ref. 12). The curves are calculated from the empirical potentials as in Fig. 12, and have been velocity averaged.

EGMSV potential, and are in excellent agreement with experimental data. In particular, the anisotropic potential provides a much better description of these properties than does the corresponding spherically averaged potential. The same is true in comparing calculated to measured total integral cross sections for $He+CO_2$. This substantiates the conclusion that these properties, as well as the total DCS measurements presented here, are sensitive not merely to some spherically symmetric "average" potential. Instead, these properties are also sensitive to anisotropic components of the intermolecular potentials. Use of the equilibrium, gas transport, and integral cross section data for $He+CO_2$, resulting in the EGMSV anisotropic potential, makes it more accurate than the $He+N_2O$ or $He+C_2N_2$ MSV potentials, for which the corresponding data are unavailable.

ACKNOWLEDGMENTS

We wish to thank Jack Kaye for persistent help in running the data reduction programs. We thank Ambassador College and University of Oklahoma computer services for generous use of their facilities. We also thank Jeanene Parker and Frank Shaw for assistance in preparing the manuscript and figures. Financial assistance for the publication of this paper was generously provided by the Natural Sciences and Engineering Research Council of Canada and by the Petroleum Research Fund administered by the American Chemical Society.

[1]For recent reviews, see (a) H. Pauly, in *Atom–Molecule Collision Theory: A Guide for the Experimentalist*, edited by R. B. Bernstein (Plenum, New York, 1979), p. 111; (b) U. Buck, Adv. Chem. Phys. **30**, 313 (1975); (c) J. P. Toennies, in *Physical Chemistry: An Advanced Treatise*, edited by H. Eyring, D. Henderson, and W. Jost (Academic, New York, 1974), Vol. 6A, p. 227.

[2]For recent examples involving scattering of light systems, see (a) C. H. Chen, P. E. Siska, and Y. T. Lee, J. Chem. Phys. **59**, 601 (1973); (b) A. Kuppermann, R. J. Gordon, and M. J. Coggiola, Faraday Discuss. Chem. Soc. **55**, 145 (1973); (c) K. M. Smith, A. M. Rulis, G. Scoles, R. A. Aziz, and V. Nain, J. Chem. Phys. **67**, 152 (1977); (d) R. A. Aziz, P. W. Riley, U. Buck, G. Manke, J. Schleusener, G. Scoles, and U. Valbusa, *ibid.* **71**, 2637 (1979).

[3](a) M. Keil, A. Kuppermann, and J. T. Slankas, Chem. Phys. Lett. **59**, 339 (1978); (b) M. Keil, J. T. Slankas, and A. Kuppermann, J. Chem. Phys. **70**, 482 (1979).

[4](a) M. Keil, J. T. Slankas, and A. Kuppermann, J. Chem. Phys. **70**, 541 (1979); (b) J. T. Slankas, M. Keil, and A. Kuppermann, *ibid.* **70**, 1482 (1979).

[5]M. Keil, G. A. Parker, and A. Kuppermann, Chem. Phys. Lett. **59**, 443 (1978).

[6]G. A. Parker and R. T Pack, J. Chem. Phys. **68**, 1585 (1978) and references therein.

[7]L. Monchick and S. Green, J. Chem. Phys. **63**, 2000 (1975).

[8](a) R. E. Olson and R. B. Bernstein, J. Chem. Phys. **49**, 162 (1968); (b) R. J. Cross, *ibid.* **52**, 5703 (1970).

[9]R. T Pack, Chem. Phys. Lett. **55**, 197 (1978).

[10]R. B. Bernstein, Adv. Chem. Phys. **10**, 75 (1966).

[11]K. G. Anlauf, R. W. Bickes, and R. B. Bernstein, J. Chem. Phys. **54**, 3647 (1971); M. Cavallini, M. G. Dondi, G. Scoles, and U. Valbusa, Chem. Phys. Lett. **10**, 23 (1971); J. M. Farrar and Y. T. Lee, *ibid.* **28**, 428 (1974).

[12]H. P. Butz, R. Feltgen, H. Pauly, and H. Vehmeyer, Z. Phys. **247**, 70 (1971).

[13](a) K. A. Reed and L. Wharton, J. Chem. Phys. **66**, 3399 (1977); (b) L. T. Tsou, D. J. Auerbach, and L. Wharton, *ibid.* **70**, 5296 (1979).

[14]For state-to-state rotationally inelastic differential cross section measurements, see U. Buck, F. Huisken, J. Schleusener, and H. Pauly, Phys. Rev. Lett. **38**, 860 (1977); W. R. Gentry and C. F. Geise, J. Chem. Phys. **67**, 5389 (1977); K. Bergmann, R. Engelhardt, U. Hefter, and J. Witt, *ibid.* **71**, 2726 (1979); J. A. Serri, A. Morales, W. Moskowitz, D. E. Pritchard, C. H. Becker, and J. L. Kinsey, *ibid.* **72**, 6304 (1980); M. Faubel, K. H. Kohl, J. P. Toennies, K. T. Tang, and Y. Y. Yung, Faraday Discuss. Chem. Soc. **73** (to be published).

[15]For integral cross section measurements with oriented molecules, see (a) H. Thuis, S. Stolte, and J. Reuss, Chem. Phys. **43**, 351 (1979); (b) U. Borkenhagen, H. Malthan, and J. P. Toennies, J. Chem. Phys. **71**, 1722 (1979); see also Ref. 13(b).

[16]For state-to-state integral cross section measurements, see, for example, P. J. Dagdigian, B. E. Wilcomb, and M. H. Alexander, J. Chem. Phys. **71**, 1670 (1979); T. A. Brunner, R. D. Driver, N. Smith, and D. E. Pritchard, *ibid.* **70**, 4155 (1979); C. R. Vidal, Chem. Phys. **35**, 215 (1978); J. A. Barnes, M. Keil, R. E. Kutina, and J. C. Polanyi, J. Chem. Phys. **72**, 6306 (1980); **76**, 913 (1982).

[17]For spectroscopic determinations of potential anisotropies, see (a) R. J. LeRoy, J. S. Carley, and J. E. Grobenstetter, Faraday Discuss. Chem. Soc. **62**, 169 (1977); (b) W. Klemperer, *ibid.* 62, 179 (1977); (c) R. E. Smalley, L. Wharton, and D. H. Levy, J. Chem. Phys. **68**, 671 (1978); (d) A. M. Dunker and R. G. Gordon, *ibid.* **64**, 354 (1976).

[18]For unresolved rotationally inelastic differential cross section measurements, see J. M. Farrar, J. M. Parson, and Y. T. Lee, Proc. 4th International Symposium on Molecular Beams, Cannes, France, 1973, p. 215; H. J. Loesch, Chem. Phys. **18**, 431 (1976); N. C. Blais, J. B. Cross, and G. H. Kwei, J. Chem. Phys. **66**, 2488 (1977).

[19]R. B. Gerber, V. Buch, and U. Buck, J. Chem. Phys. **72**, 3596 (1980).

[20](a) For a recent, complete survey of approximation methods, see D. J. Kouri, in *Atom–Molecule Collision Theory: A Guide for the Experimentalist*, edited by R. B. Bernstein (Plenum, New New York, 1979), p. 301; (b) For an important and useful additional method, see A. E. DePristo, S. D. Augustin, R. Ramaswamy, and H. Rabitz, J. Chem. Phys. **71**, 850 (1979).

[21](a) S. Green and L. Monchick, J. Chem. Phys. **63**, 4198 (1975); (b) S. Green, L. Monchick, R. Goldflam, and D. J. Kouri, *ibid.* **66**, 1409 (1977).

[22]R. B. Walker and J. C. Light, Chem. Phys. **7**, 84 (1975).

[23]P. McGuire, Chem. Phys. **8**, 231 (1975).

[24]J. M. Bowman and S. C. Leasure, J. Chem. Phys. **66**, 288 (1977).

[25]T. P. Tsein, G. A. Parker, and R. T Pack, J. Chem. Phys. **59**, 5373 (1973); R. T Pack, *ibid.* **66**, 1557 (1977).

[26]Y. Shimoni and D. J. Kouri, J. Chem. Phys. **66**, 2481 (1977); D. J. Kouri and Y. Shimoni, *ibid.* **67**, 86 (1977).

[27]V. Khare, J. Chem. Phys. **67**, 3897 (1977).

[28]R. Schinke and P. McGuire, J. Chem. Phys. **71**, 4201 (1979).

[29]R. T Pack, J. Chem. Phys. **60**, 633 (1974).

[30]P. McGuire and D. J. Kouri, J. Chem. Phys. **60**, 2488 (1974). (1974).

[31](a) D. Secrest, J. Chem. Phys. **62**, 710 (1975); (b) V. Khare, *ibid.* **68**, 4631 (1978).

[32]J. A. Blazy, B. M. DeKoven, T. D. Russell, and D. H. Levy, J. Chem. Phys. **72**, 2439 (1980).

[33]R. T Pack and R. K. Preston (unpublished work).

[34]G. Rotzoll and A. Lübbert, J. Chem. Phys. **71**, 2275 (1979).

[35]J. B. Anderson and J. B. Fenn, Phys. Fluids **8**, 780 (1965).

[36]It is convenient to refer to $I(\theta)$ as a laboratory DSC in arbitrary units. However, $I(\theta)$ is really a signal intensity. To transform it into such a laboratory DCS requires multiplica-

tion by the laboratory velocity of the scattered beam (which is a function of θ), since the mass spectrometer is a number density detector.
[37]D. W. Marquardt, J. Soc. Indust. Appl. Math. 11, 431 (1963).
[38]N. R. Draper and H. Smith, *Applied Regression Analysis* (Wiley, New York, 1966).
[39]Our M^2SV potential is somewhat similar to the MMSV part of the ESMMSV potential form proposed by A. L. J. Burgmans, J. M. Farrar, and Y. T. Lee, J. Chem. Phys. 64, 1345 (1976). However, we join the two Morse functions at σ, rather than at r_m [Ref. 3(b)].
[40]G. Simmons, R. G. Parr, and J. M. Finlan, J. Chem. Phys. 59, 3239 (1973).
[41]R. W. Bickes and R. B. Bernstein, Chem. Phys. Lett. 26, 457 (1974). We use the long-range behavior to fix two of the SPFD coefficients by smoothness conditions, rather than the reverse [Ref. 3(b)].
[42]M. Keil and A. Kuppermann, J. Chem. Phys. 69, 3917 (1978).
[43]J. M. Parson and Y. T. Lee, Entropie 42, 146 (1971). Our MSV potential differs in the choice of spline points [Ref. 3(b)].
[44]J. Hepburn, G. Scoles, and R. Penco, Chem. Phys. Lett. 36, 451 (1975); R. Ahlrichs, R. Penco, and G. Scoles, Chem. Phys. 19, 119 (1977).
[45]J. M. Hutson and B. J. Howard, Mol. Phys. 43, 493 (1981).
[46]C. Douketis, G. Scoles, S. Marchetti, M. Zen, and A. J. Thakkar, J. Chem. Phys. 76, 3057 (1982); K. T. Tang and J. P. Toennies, *ibid.* 68, 5501 (1978).
[47]A. D. Buckingham, R. L. Disch, and D. A. Dummur, J. Am. Chem. Soc. 90, 3104 (1968).
[48]For a description of these potentials and their ability to fit DCS measurements of isotropic interactions, see Refs. 42 and 44.
[49]For $He+CO_2$, we use the coefficients of R. T Pack, J. Chem. Phys. 64, 1659 (1976). For $He+N_2O$, C_2N_2 the dispersion constants were determined using the relations $C_6^x(0) = C_6^{CO_2}(0)\,\alpha^x/\alpha^{CO_2}$ where $x = N_2O, C_2N_2$ and α is the static dipole polarizability (Ref. 50). The $C_6(2)$, $C_8(0)$, and $C_8(2)$ coefficients were calculated using expressions of this reference which use the polarizability anisotropies (Refs. 50 and 51).
[50]J. O. Hirschfelder, C. F. Curtiss, and R. B. Bird, *Molecular Theory of Gases and Liquids* (Wiley, New York, 1954), p. 950.
[51]N. J. Bridge and A. D. Buckingham, Proc. R. Soc. Edinburgh Sect. A 295, 334 (1966).
[52]For other simple but flexible anisotropic potential parametrizations suitable for fitting experimental data, see R. A. LaBudde and R. B. Bernstein, J. Chem. Phys. 55, 5499 (1971); see also Ref. 9.
[53]C. H. Becker, P. W. Tiedemann, J. J. Valentini, Y. T. Lee, and R. B. Walker, J. Chem. Phys. 71, 481 (1979).
[54]Further examples include S. Green and P. Thaddeus, Astrophys. J. 205, 766 (1976); M. H. Alexander, J. Chem. Phys. 67, 2703 (1977).
[55](a) G. A. Parker, R. L. Snow, and R. T Pack, J. Chem. Phys. 64, 1668 (1976); (b) C. L. Stroud and L. M. Raff, *ibid.* 72, 5479 (1980).
[56]J. Brewer, Tech. Rep. AD 663448 (1967). Available from the Clearinghouse for Federal Scientific and Technical Information.
[57]T. L. Cottrell, R. A. Hamilton, and R. P. Tambinger, Trans. Faraday Soc. 52, 156, 1310 (1956).
[58]T. N. Bell and P. J. Dunlop, Chem. Phys. Lett. 84, 99 (1981).
[59]A. E. Loiko, B. A. Ivakin, and P. E. Suetin, Zh. Tekh. Fiz. 44, 682 (1974) [English translation: Soviet Phys. Tech. Phys. 19, 434 (1974)].
[60]S. J. Harris, K. C. Janda, S. E. Novick, and W. Klemperer, J. Chem. Phys. 63, 881 (1975).
[61]Reference 50, pp. 153–4.
[62]L. Monchick, K. S. Yun, and E. A. Mason, J. Chem. Phys. 39, 654 (1963).
[63]I. Nigata and T. Hasegawa, J. Chem. Eng. Jpn. 3, 143 (1970).
[64]S. C. Saxena and E. A. Mason, Mol. Phys. 2, 379 (1959).
[65]B. A. Ivakin and P. E. Suetin, Zh. Tekh. Fiz. 34, 1115 (1964) [English translation: Sov. Phys. Tech. Phys. 9, 866 (1964)].
[66]N. D. Kosov and A. F. Bogatyrev, Teplofiz. Massoperenos 7, 497 (1968); A. G. Karpushin and N. D. Kosov, Fizika (Alma-Ata) 1, 127 (1970).
[67]J. Kestin and S. T. Ro, Ber. Bunsenges. Phys. Chem. 78, 20 (1974); see also R. DiPippo, J. Kestin, and K. Oguchi, J. Chem. Phys. 46, 4758 (1967).
[68]E. B. Smith and A. R. Tindell, Faraday Discuss. Chem. (to be published).
[69]C. Douketis, M. Keil, G. A. Parker, and G. Scoles (to be published).